$CN)_2$. It does not appear necessary to postulate an appreciable geometric distortion of the NCCN molecule to reasonably account for the large induced moment.

It is noteworthy that NCCN possesses a very low lying π_u^* orbital and suggests that a molecular orbital picture of NCCN complexes may be insightful. The lowest lying $\pi-\pi^*$ electronic transition in NCCN involves an excited state 33 290 cm^{-1} above the ground state.[30,31] The lowest lying electronic states in HCN and CH_3CN are at 52 260 and 55 000 cm^{-1}, respectively.[32] The overlap of the two neighboring CN π^* orbitals apparently produces a much lower energy molecular orbital, $2\pi_u^*$. This orbital is of the proper symmetry to interact with the lone pair on the N atom of either NH_3 or NCCN. This picture is consistent with the molecular orbital picture that emerges from the calculations of McLean and Yoshimine.[21] We hope in the near future to examine the geometry of the H_2O-NCCN complex to compare the structure and internal rotation to that of the H_2O-CO_2 system.

The weak complexes of NCCN belie our original idea that NCCN chemistry would be analogous to that of HCN without the H end. The central carbons are active, and NCCN complexes that do interact on the nitrogen end are much less tightly bound than the corresponding HCN and NH_3 complexes. The N-F bond distance in HF-NH_3, HF-NCH, and HF-NCCN are 2.70, 2.805, and 2.863 Å, respectively.[33] Clearly the nitrogen lone pair is much less active on a nitrogen atom that is sp hybridized than one that is sp^3 hybridized. What is surprising is that the bond distance is so much longer (0.06 Å) in HF-NCCN than in HF-NCH. One might argue that the short HF-NCH bond length results from strong dipole-dipole coupling absent in HF-NCCN. However, electrostatic models consistently show that one cannot make bonding arguments from only the lowest order multipole. The molecular orbital picture developed by McLean and Yoshimine may hold a clue to the comparatively weak bond in HF-NCCN. One of the nonbonding lone pairs occupies a σ orbital that is composed mainly of s and p orbitals from the two interior carbons. Thus, the lone pairs may be less accessible in NCCN than in HCN.

Acknowledgment. This work was supported by the National Science Foundation.

(30) Woo, S. C.; Liu, T. K. *J. Chem. Phys.* **1937**, *5*, 161.
(31) Callomon, J. H.; Davey, A. B. *Proc. Phys. Soc., London* **1963**, *82*, 335.
(32) Herzberg, G. *Molecular Spectra and Molecular Structure*; D. Van Nostrand: New York, 1966; Vol. III, pp 588, 631.
(33) Novick, S. E.; Leopold, K. R.; Klemperer, W. In *Atomic and Molecular Clusters*; Bernstein, E. R., Ed.; Elsevier: New York, 1990; pp 359-391.

State-Resolved Vibrational-Energy-Transfer Channels from S_1 0^0 *p*-Difluorobenzene in Collision with He and Ar

David L. Catlett, Jr.,† and Charles S. Parmenter*

Department of Chemistry, Indiana University, Bloomington, Indiana 47405 *(Received: October 8, 1990)*

State-to-state vibrational energy transfer (VET) from the zero-point level of S_1 *p*-difluorobenzene (pDFB) vapor at 300 K has been studied for single collisions with He and Ar. As seen in other polyatomic VET studies, high selectivity occurs among possible channels in this 30-mode molecule. The competition among VET channels has a marked dependence on collision partner. Large absolute rate constants are measured for total VET from the 0^0 level and for the dominant state-to-state channels. The total VET rate constant is 1.6×10^6 $Torr^{-1}$ s^{-1} for He and 1.8×10^6 $Torr^{-1}$ s^{-1} for Ar, roughly one-fifth hard sphere for each. The transfer channels involve quantum changes in only the two lowest frequency modes, ν_{30} = 119 cm^{-1} and ν_8 = 173 cm^{-1}. The channel $0^0 \rightarrow 30^1$ dominates VET for each gas. With Ar collisions, for which five channels have been measured, it accounts for about 90% of the transfer. With He, it is 60% of the transfer, competing with the $0^0 \rightarrow 8^1$ channel that has about 30%. The absolute rate constants for the two He + pDFB channels are within a factor of 2 of values calculated by Clary using three-dimensional quantal scattering theory. A treatment of the SSH-T model accounts well for the competition between VET channels as well as for the differences between collision partners. The account is in the familiar form of propensity rules, similar to those developed earlier for VET in S_1 benzene, aniline, and pyrazine.

Introduction

Collisional vibrational energy transfer (VET) in polyatomics remains along the central problems of chemical physics. The fact that one of the earliest applications of lasers to chemical physics involved state-resolved VET studies attests to its venerable nature.[1] Recent applications of new laser techniques underscore the persistent interest.[2]

One of the most productive routes to the study of VET is based on the optical pump-dispersed fluorescence approach so long used for diatomics in 300 K thermal systems.[3] When practical tunable UV pumps were developed,[4] the method became suitable also for polyatomics. Its first application, involving the 30-mode molecule benzene,[5] showed immediately the advance in VET resolution provided by the method. From an initial level selected among several possibilities, one could obtain absolute state-to-state cross sections for every important VET channel. The VET flow pattern is defined by this set of rate constants. If the constants are normalized among themselves, one obtains the branching ratios

* To whom correspondence should be addressed.
† Present address: Texas Instruments, Inc., 13353 Floyd Road, P.O. Box 655012, Mail Stop 374, Dallas, TX 75265.

(1) (a) Yardley, J. T.; Moore, C. B. *J. Chem. Phys.* **1966**, *45*, 1066. (b) Hocker, L. O.; Kovacs, M. A.; Rhodes, C. K.; Flynn, G. W.; Javan, A. *Phys. Rev. Lett.* **1966**, *17*, 233.
(2) (a) Hetzler, J.; Millot, G.; Steinfeld, J. I. *J. Chem. Phys.* **1989**, *90*, 5434. (b) Zhu, L.; Hershberger, J. F.; Flynn, G. W. *J. Chem. Phys.* **1990**, *92*, 1687.
(3) The method had its genesis with I_2: Wood, R. W. *Philos. Mag.* (*Ser. 6*) **1911**, *21*, 309. Franck, J.; Wood, R. W. *Philos. Mag.* (*Ser. 6*) **1911**, *21*, 314; *Verh. Dtsch. Phys. Ges.* **1911**, *13*, 78. I_2 has also played a prominent role in the continuing evolution of the technique: Steinfeld, J. I. *J. Phys. Chem. Ref. Data* **1984**, *13*, 445. Krajnovich, D. J.; Butz, K. W.; Du, H.; Parmenter, C. S. *J. Chem. Phys.* **1989**, *92*, 7705.
(4) Two types of pumps capable of exciting S_1 single vibronic levels (SVL) were required. Tunable CW sources led to SVL fluorescence spectra containing the level population information needed for VET: Parmenter, C. S.; Schuyler, M. W. *Transitions Non Radiat. Mol., Reun. Soc. Chim. Phys., 20th, 1969* **1970**, 29 (*J. Chim. Phys. Suppl.* **1969-70**). Tunable nanosecond sources provided the SVL fluorescence lifetimes needed for conversion of relative to absolute rate constants: Gelbart, W. M.; Freed, K. F.; Jortner, J.; Rice, S. A. *Chem. Phys. Lett.* **1970**, *6*, 345. Ware, W. R. In *Creation and Electron of the Excited State*; Lamola, A. A., Ed.; Marcel Dekker: New York, 1971.

0022-3654/91/2095-2864$02.50/0 © 1991 American Chemical Society

from a given level. Alternatively, the constants can be normalized to a separately measured rate constant for total VET from the initial level to give the fraction of transfer occurring to each final state. It is still difficult to find another method that gives such complete and well-resolved views of single-collision VET in vibrationally complex molecules.

In addition to benzene, S_1 flow patterns from at least several levels have now been characterized in six molecules,[6,7] half by Rice and co-workers,[8] who also have made numerous developments in both the experimental and theoretical techniques.

In every case, the data reveal that the VET is governed by strong propensity rules. The rules express themselves most directly by severely limiting the state-to-state transfer. Qnly a few channels among the many possibilities are used. Thus, single-collision VET in S_1 polyatomics turns out to a relatively simple phenomenon, even in the midst of a complicated vibrational level structure.

Beyond this simplification, the rules have sufficient variability among molecules that no single scheme can yet tie them all together. Three molecules, however, form a special set. In benzene, aniline,[9,10] and pyrazine,[11] the VET similarities far exceed the differences. As an example, McDonald and Rice[12] have shown that a variant of the propensity rules developed for benzene can give at least a qualitative account of state-to-state VET in all three "aromatics".

In this report, we begin a description of single-collision VET in another aromatic, *p*-difluorobenzene (pDFB). The molecule has been chosen because of both experimental and molecular virtues. On the experimental side, the molecule has strong S_1–S_0 absorption and emits with high quantum yields. Both the yields and collision-free lifetimes are known for many S_1 levels.[13] The absorption and single vibronic level (SVL) emission spectroscopy are well understood.[14,15] The SVL spectra are discretely structured for S_1 levels with ϵ_{vib} as high as 1500 cm^{-1}. The S_1 vibrational level structure is known for the first 1000 cm^{-1} of vibrational energy, and many opportunities exist to pump SVLs within this region. Finally, the molecule is stable and has a 60 Torr vapor pressure at 300 K.

The experimental assets have generated some of the molecular motivations. One is that much is known about intramolecular vibrational redistribution (IVR) in collision-free S_1 pDFB as a result of chemical timing studies.[16] Those studies identify the lowest S_1 mode, ν_{30}, as particularly effective in accelerating IVR.[17] This finding is consistent with spectroscopic observations of ν_{30} activity in mixing among S_1 levels.[18,19] Conventional wisdom, derived in part from the aromatic single-collision studies discussed above,[7] suggests that ν_{30} will be also an active mode in collisional VET,[20] an issue we explore here. The expectations have been fulfilled in the extreme by the pioneering crossed molecular beam studies of collisional VET in S_0 polyatomics by Gentry and coworkers.[21] They find that ν_{30} is in fact the *only* active mode in S_0 pDFB.

A second issue concerns vibrational predissociation (VP) of the S_1 pDFB–Ar van der Waals complex. This process has been studied with state-to-state resolution, both experimentally[22-24] and theoretically.[25] Since the VP can be considered as vibrational energy flow in a half-collision, an interesting question concerns the extent to which the full collisional characteristics are related.

Explorations of collisional VET also exist within the ground electronic state. They derive from two novel S_0 studies. One is the crossed-beam effort mentioned above. The second is from simulated emission pumping of S_0 levels.[26] Both will be discussed here or elsewhere in conjunction with our pDFB S_1 results.

Additionally, the pDFB system is amenable to modern three-dimensional quantal scattering theory.[27] This new theoretical development ends a long period of dormancy for the quantal theory of polyatomic VET, and it provides additional motivations to obtain good experimental data.

These issues aside, S_1 pDFB provides a highly instructive polyatomic VET system in its own right. Among the aromatics so far studied at 300 K, pDFB with eight fundamentals below 500 cm^{-1} presents easily the most complex S_1 vibrational level structure in which VET can actually be probed. The possibilities for competition among state-to-state channels involving low-frequency modes are intrinsically rich. Additionally, the initial S_1 levels from which VET can be studied encompass fundamentals, overtones, or combinations of at least four and possibly six modes. A rather comprehensive view of state-to-state single-collision VET should emerge.

These expectations have been largely fulfilled.[28] Some of our findings have been described in brief reports.[7,20] In this paper we begin the detailed presentation of our results. We here describe VET from the S_1 zero-point level occurring with two collision partners, He and Ar. There is a difference for these gases that is surprising in the context of some past experience. We also present a development of propensity rules that will be used to describe not only the 0^0 results but later also the VET from higher S_1 levels.[28]

The rules warrant further comment in this introduction. A large ensemble of aromatic data is modeled with an essentially uniform set of propensity rules. Reviews[7,8] of those data and their modeling are available. The propensity rules are based on the venerable SSH-T model[29,30] of polyatomic VET that for a long time was the only theoretical treatment with both generality and success. Recently, Clary has introduced a modern three-dimensional quantal scattering treatment for polyatomics and has made detailed calculations for VET in the pDFB + He system.[27] We give a brief discussion of his results later as they pertain to our data.

The success of Clary's method, not only with pDFB but also with VET in other polyatomic systems,[31] is an exciting development. These complicated VET processes can now be approached by quantal calculations that treat the problem from first principles with satisfying realism.

In view of this theory, one might assume that the SSH-T model,

(5) Parmenter, C. S.; Tang, K. *Chem. Phys.* **1978**, *27*, 127.
(6) Aniline, pyrazine, *s*-tetrazine, difluorodiazirine, glyoxal, and the diradical CF_2. References for all and a review of all except *s*-tetrazine are given in ref 7.
(7) Krajnovich, D. K.; Parmenter, C. S.; Catlett, D. L., Jr. *Chem. Rev.* **1987**, *87*, 237.
(8) Rice, S. A. *Adv. Chem. Phys.* **1981**, *47* (2), 237.
(9) (a) Chernoff, D. A.; Rice, S. A. *J. Chem. Phys.* **1979**, *70*, 2521. (b) Vandersall, M.; Chernoff, D. A.; Rice, S. A. *J. Chem. Phys.* **1981**, *74*, 488. (c) Cameron, S. M.; Vandersall, M.; Rice, S. A. *J. Chem. Phys.* **1981**, *75*, 1046.
(10) Pineault, R. L.; Crackel, R. L.; Hedstrom, J. F.; Struve, W. S. *J. Chem. Phys.* **1984**, *80*, 5545.
(11) McDonald, D. B.; Rice, S. A. *J. Chem. Phys.* **1981**, *74*, 4893.
(12) McDonald, D. B.; Rice, S. A. *J. Chem. Phys.* **1981**, *74*, 4907.
(13) (a) Guttman, C.; Rice, S. A. *J. Chem. Phys.* **1974**, *61*, 661. (b) Volk, L. J.; Lee, E. K. C. *J. Chem. Phys.* **1977**, *67*, 236.
(14) Coveleskie, R. A.; Parmenter, C. S. *J. Mol. Spectrosc.* **1981**, *86*, 86.
(15) Knight, A. E. W.; Kable, S. H. *J. Chem. Phys.* **1988**, *89*, 7139.
(16) Holtzclaw, K. W.; Parmenter, C. S. *J. Chem. Phys.* **1986**, *84*, 1099.
(17) Holtzclaw, K. W.; Parmenter, C. S. *J. Chem. Phys.* **1985**, *82*, 5283.
(18) Kable, S. H.; Lawrance, W. D.; Knight, A. E. W. *J. Phys. Chem.* **1982**, *86*, 1244.
(19) Fujii, M.; Ebata, T.; Mikami, N.; Ito, M.; Kable, S. H.; Lawrance, W. D.; Parsons, T. B.; Knight, A. E. W. *J. Phys. Chem.* **1984**, *88*, 2937.
(20) Catlett, Jr., D. L.; Holtzclaw, K. W.; Krajnovich, D.; Moss, D. B.; Parmenter, C. S.; Lawrance, W. D.; Knight, A. E. W. *J. Phys. Chem.* **1985**, *89*, 1577.
(21) Hall, G.; Giese, C. F.; Gentry, R. W. *J. Chem. Phys.* **1985**, *83*, 5343.
(22) Butz, K. W.; Catlett, Jr., D. L.; Ewing, G. E.; Krajnovich, D.; Parmenter, C. S. *J. Phys. Chem.* **1986**, *90*, 3522.
(23) O, H.-K.; Parmenter, C. S.; Su, M.-C. *Ber. Bunsen-Ges. Phys. Chem.* **1988**, *92*, 253.
(24) Jacobson, B. A.; Humphrey, S.; Rice, S. A. *J. Chem. Phys.* **1988**, *89*, 5624.
(25) Tiller, A. R.; Peet, A. C.; Clary, D. C. *Chem. Phys.* **1989**, *129*, 125.
(26) (a) Kable, S. H.; Knight, A. E. W. *J. Chem. Phys.* **1990**, *93*, 3151. (b) Kable, S. H.; Knight, A. E. W. *J. Chem. Phys.* **1987**, *86*, 4709. (c) Thoman, J. W., Jr.; Kable, S. H.; Rock, A. B.; Knight, A. E. W. *J. Chem. Phys.* **1986**, *85*, 6234.
(27) Clary, D. C. *J. Chem. Phys.* **1987**, *86*, 813.
(28) Catlett, Jr., D. L. Ph.D. Thesis, Indiana University, 1985.
(29) Schwartz, R. N.; Slawsky, Z. I.; Herzfeld, K. F. *J. Chem. Phys.* **1952**, *20*, 1591. (b) Schwartz, R. N.; Herzfeld, K. F. *Ibid.* **1954**, *22*, 767.
(30) Tanczos, F. I. *J. Chem. Phys.* **1956**, *25*, 439.
(31) Clary, D. C. *J. Phys. Chem.* **1987**, *91*, 1718.

justifiably termed "crude",[32] would quickly fade from view. In fact, theoretical work with the model stopped long ago. In view of the model's inability to account for the magnitudes of the larger polyatomic VET rate constants, one might expect experimentalists to abandon it as well. Until the new scattering calculations become both more accessible and abundant, however, the SSH-T approach remains useful, particularly for propensity rules. As we shall show, the model is especially good in replicating the pDFB flow patterns from 0^0 and higher levels. Its success further infers that the model incorporates at least the most essential elements of the physics governing the *competition* among state-to-state channels. In turn, the transparency of the model allows us to gain insights into the operation of large-molecule collisional VET. Thus, we spend some efforts in exploring the adaption of SSH-T procedures to the pDFB + Ar and pDFB + He systems.

Experimental Procedures

Radiation from a Quanta Ray Nd:YAG pumped pulsed dye laser with Exciton Coumarin 500 dye was used as an excitation source. The visible laser output was frequency-doubled into the UV region by an INRAD temperature tuned ADP crystal giving 5-ns pulses at 10 Hz with a 2-cm^{-1} band-pass.

Exciting light tuned to the 0_0^0 absorption band maximum was passed through a cross-shaped fluorescence cell with quartz windows. Fluorescence collected at right angles to the laser was imaged into a Spex 0.85-m double monochromator with quartz lenses.

The dispersed fluorescence was monitored by an EMI 9789 photomultiplier typically operated at −1800 V. Its signal was processed with channel A of a PAR boxcar averager operated in the A/B ratio mode with an aperture duration of 50 ns. Channel B was the output of a RCA 1P28 reference PMT that monitored the UV laser power. The boxcar was triggered by a photodiode looking at the laser pulse.

pDFB purchased from Aldrich Chemical Co. was degassed several times before use. Ar and He were leaked into the cell from large bulbs on the vacuum line. All chemicals were supplied with 99+% stated purity. Care was taken to ensure complete gas mixing in the fluorescence cell. Cell pressures to 10 Torr were monitored with an MKS Baratron Model 144 capacitance manometer. Higher pressures were monitored with a Wallace-Tiernan Bourdon gauge.

More details of the equipment and procedures are given elsewhere.[28,33,34]

Results

The state-to-state vibrational energy-transfer rate constants derive from new fluorescence bands that grow in pDFB fluorescence spectra upon addition of foreign gas. The derivation involves several steps, the first of which is the identification of growth bands used to monitor the relative populations of S_1 levels. Second, procedures must be introduced for quantitative band intensity measurements. Third, methods must be developed to relate accurately these intensities to relative level populations. We finally need a realistic kinetic model, with evaluation of specific rate constants, to transform the relative level populations into the state-to-state rate constants.

The means to achieve these tasks were detailed in our previous benzene VET study.[5] The pDFB procedures are essentially the same, but some changes in details are needed.

Identification of Collisionally Populated Levels. With more than 120 S_1 vibrational levels lying within $4kT$ of the 0^0 level and hence accessible to thermal collisions, success might seem improbable. Prior experience with aromatics suggests,[7] however, that large cross sections will involve only a few levels and that those levels will be within about $2kT$ of the 0^0 level. Accordingly, we search initially for fluorescence from the 13 levels that lie within 438 cm^{-1} of 0^0. The 13 levels are given in Table I. They involve seven fundamentals plus their overtones and combinations.

TABLE I: Positions of the Most Intense Fluorescence Band[a] from Each S_1 pDFB Level up to 438 cm^{-1}

fluorescing level	E_{vib}, cm^{-1}	transition	band maximum position, cm^{-1} absolute	band maximum position, cm^{-1} displacement from 5_1^0	labeled region of spectrum[b]
0^0	0	5_1^0	35981.0	0	not shown
30^1	119	$5_1^0 30_1^1$	35943.2	−37.8	A
8^1	173	$5_1^0 8_1^1$	35728[c]	−253[c]	D
30^2	238	$5_1^0 30_2^2$	35905.5	−75.5	B
17^1	275	$5_1^0 17_1^1$	35881.0	−100.0	C
$8^1 30^1$	292	$5_1^0 8_1^1 30_1^1$	35687[d]	−293[d]	E
8^2	346	$6_1^0 8_2^2$	35893[e]	−84[e]	B
22^1	353	$5_1^0 22_1^1$	35984.5	+3.5	not shown
30^3	357	$5_1^0 30_1^1$	35867.7	−113.3	C
27^1	391	$5_1^0 27_1^1$	35938.0	−43.0	A
$17^1 30^1$	394	$5_1^0 17_1^1 30_1^1$	35843.2	−137.8	not shown
6^1	410	$5_1^0 6_1^1$	35941.7	−39.3	A
$8^1 30^2$	411	$5_1^0 8_1^1 30_2^2$	35647[e]	−334[e]	not shown
29^1	438	$5_1^0 29_1^1$	35911.0	−70.0	B

[a] The band from 8^2 is an exception. It is not the most intense from that level. [b] See Figures 1 and 2. [c] Uncertainty of ±1 cm^{-1}. The displacement 5_1^0–$5_1^0 8_1^1$ is observed to be different than that for 0^0–8_1^1 (−246 cm^{-1}). [d] Uncertainty of ±1 cm^{-1}. The displacement $5_1^0 8_1^1$–$5_1^0 8_1^1 30_1^1$ is observed to be −40.5 cm^{-1}. [e] Uncertainty of ±5 cm^{-1}.

Such a search identifies all of the growth bands with Ar collisions and all but three bands with He collisions. Those He bands are small and represent minor VET channels. They remain unidentified.

A level reached by VET will have a small population relative to the initially pumped 0^0 level, and only their most intense emission bands will be observed. For any level in Table I, two bands will dominate the fluorescence spectrum.[14] For some level X^n (n quanta of ν'_x), the sequence band X_n^n and its ν_5 progression member $5_1^0 X_n^n$ are the most intense, occurring with roughly equal intensities. Similarly, from a combination level $X^n Y^m$, we would observe most readily the bright bands $X_n^n Y_m^m$ and $5_1^0 X_n^n Y_m^m$.

Some sequence bands fall near the 0_0^0 band and have interference from scattered exciting light. On the other hand, the progression bands occur in a nearly clear region of 0^0 fluorescence lying in the 500-cm^{-1} span 36000–35500 cm^{-1}. This region is approximately bounded by the 5_1^0 and 3_1^0 bands of 0^0 emission.[14] Most of our data come from this region.

Table I lists the specific transitions and their positions for the 13 possible VET levels. For discussion, the listed band displacement from the 5_1^0 band proves most convenient.

Bands from 22^1 and 8^2 are special cases. The bright bands from 22^1 are always almost coincident with a bright band from 0^0. The 3.5-cm^{-1} separation[14,35] of the 22_1^1 sequence from corresponding 0^0 features makes 22^1 monitoring impossible. We will argue later, however, that 22^1 is not a significant VET participant. The band $6_1^0 8_2^2$ listed for 8^2 is not the most intense, being about 4 times weaker than the dominant band $5_1^0 8_2^2$. The latter occurs in a region of substantial interference from the 0^0 transitions 3_1^0 and $5_1^0 6_1^0$.

Figure 1 shows examples of a 120-cm^{-1} segment of fluorescence lying just to the red of 5_1^0. Table I growth bands with displacements not exceeding −120 cm^{-1} would appear in these spectra. The calculated positions of all Table I emission bands that fall in the region are designated in the figure by the emitting level.

The intensity maximum in region A occurs near the expected positions of fluorescence from 6^1 and 30^1. The calculated band maxima have a separation of 1.5 cm^{-1}, too close to resolve. The fluorescence band 6_0^1 was sought in another spectral region as an unambiguous flag for 6^1 emission. No distinct band occurred for

(32) Rice, S. A. *J. Phys. Chem.* **1986**, *90*, 3063.
(33) Longfellow, R. J.; Moss, D. B.; Parmenter, C. S. *J. Phys. Chem.* **1988**, *92*, 5438.
(34) Coveleskie, R. A.; Dolson, D. A.; Parmenter, C. S. *J. Phys. Chem.* **1985**, *89*, 655.
(35) Cvitas, T.; Hollas, M. J. *Mol. Phys.* **1970**, *18*, 793.

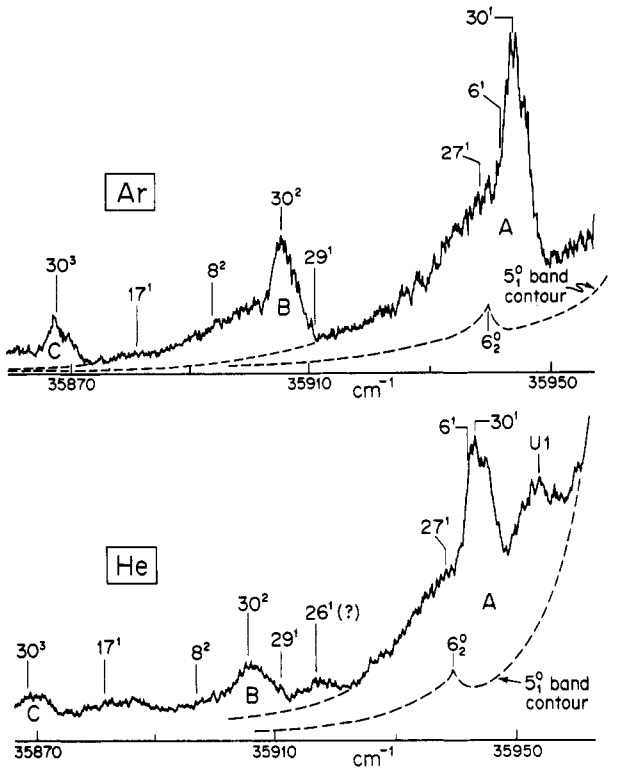

Figure 1. A segment of the fluorescence spectrum from 10 mTorr of pDFB with pumping of 0^0_0 in the presence of 13 Torr of Ar or 20 Torr of He. The emission level labels identify the expected position of band maxima listed in Table I. Dashed lines extrapolate the expected contours of the 5^0_1, 6^0_2, 30^1_1, and 30^2_2 bands under these fluorescence conditions.

either Ar or He as collision partners.[28] Thus, the level 30^1 is responsible for the big emission band in region A, with 6^1 contributing less than 1%.

In the midst of numerous possibilities, the only securely identified growth bands with Ar are those from the levels 30^1, 30^2, and 30^3. Additional bands occur with He, the most prominent of which is unidentified (marked U1), but it contains less than 10% of the region A intensity. Emission that might be from 26^1 and 17^1 also occurs with He (but not Ar), but we have not been able to monitor these intensities quantitatively. The level 26^1 is not included in Table I since it lies at 574 cm^{-1}.

Figure 2 contains similar presentations for added Ar or He in the spectral region 240–300 cm^{-1} to the red of 5^0_1. Only two of the Table I levels would generate intense emission bands in these regions, and the fluorescence from each, 8^1 and 8^130^1, is unmistakable for both added gases. The Ar and He spectra have markedly different band contours, most probably a consequence of different rotational energy transfer accompanying the VET. As in region A, the He spectrum also contains a small unidentified band, marked U.

We note that the fluorescence bands from 8^1 and 8^130^1 with displacements from 5^0_1 of -253 ± 1 and -293.5 ± 1 cm^{-1}; respectively, were at first puzzling because they were 7 cm^{-1} away from the calculated sequence displacements. The band were tentatively assigned as $5^0_18^1_1$ and $5^0_18^1_130^1_1$ because their 40.5-cm^{-1} separation corresponded exactly to the interval between 8^1_1 and $8^1_130^1_1$ in absorption and because no alternative assignments could be found. Direct excitation of 8^1 via the 8^1_1 hot band has shown that the position of $5^0_18^1_1$ fluorescence is that of the -253-cm^{-1} growth band to within ± 1 cm^{-1}, confirming the assignment.[28]

Quantitative Fluorescence Band Intensity Measurements. The intensity of the 5^0_1 band, $I_f(0^0)$, in the 0^0 SVL fluorescence spectrum was chosen as a monitor of the relative 0^0 vibrational population as collisional conditions were changed. Since only the decay of the 0^0 level was sought, the monochromator was used with a 40-cm^{-1} band-pass. About 80% of the rovibrational band contour is encompassed. There are no significant intensity contributions by fluorescence from S_1 levels populated by VET.

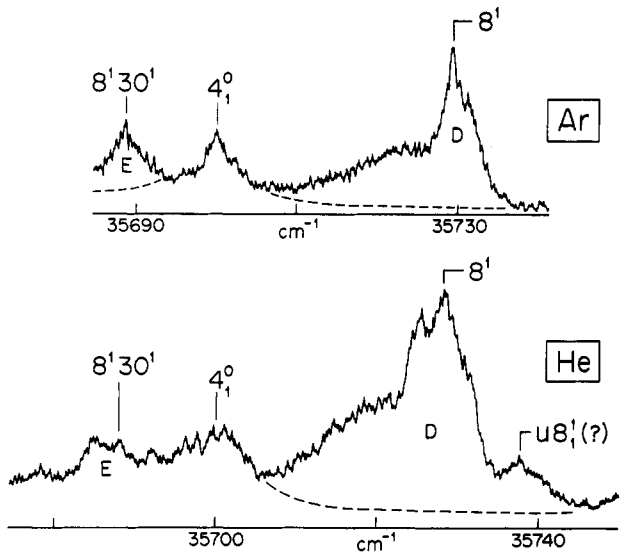

Figure 2. A segment of the fluorescence spectrum from 10 mTorr of pDFB with pumping of 0^0_0 in the presence of 13 Torr of Ar or 20 Torr of He. The dashed lines extrapolate the expected contributions of 0^0_0 emission to the spectrum. The calculated positions of maxima from those growth bands in Table II that fall in this region are shown by the level designations.

The intensity of the growth bands identified above were always monitored relative to that of 5^0_1 or relative to other growth bands. The intensities were measured by integrating areas under bands. For this purpose, spectra were obtained with monochomator resolution usually in the range of 1.5–3 cm^{-1}. Since spectral features were often separated by as much as 40 cm^{-1}, reasonable approximations to rotational contours could be perceived. Corrections based on calculated Franck–Condon factors were made for interferences by small bands from the 0^0 level.[28]

Conversion of Band Intensities to Level Populations. The kinetic model used to obtain rate constants from fluorescence data (see below) is formulated in terms of level populations. The conversion of band intensities to populations is relatively secure because we use relative rather than absolute populations. The most uncertain conversion factors ultimately disappear.

As convenient, the intensity of a band is designated by either $I_f(X^n_m)$ indicating the specific transition or $I_f(X^n)$ describing the emitting level. $I_f(X^n_m)$ is related to the population of the emitting level $[B(X^n)]$ by

$$I_f(X^n_m) = K\phi(X^n)\ \mathrm{FC}(X^n_m)\ \nu^3(X^n_m)[\mathrm{B}(X^n)]$$

We collect the constants together with the symbol $A(X^n_m)$ so that

$$I_f(X^n_m) = A(X^n_m)[\mathrm{B}(X^n)]$$

Within $A(X^n_m)$, the constant K is an ensemble of constants associated with the fluorescence detection including an overall wavelength response function. K can be safely assumed identical for all monitored fluorescence bands in our limited wavelength region. We judge from reported[13] fluorescence emission yields $\phi(X^n)$ and lifetimes that $\phi(X^n)$ is essentially the same for all levels under consideration here. $\nu(X^n_m)$ is the transition frequency. $\mathrm{FC}(X^n_m)$ is the Franck–Condon factor and hence the fraction of emission from X^n that occurs in the band.

In the use of $I_f(X^n_m)$, the most convenient quantity is the ratio of band intensities from two vibrational states, say X^n and Y^l, that would be monitored by the emission bands X^n_m and Y^l_k. Intensities and populations now appear as

$$\frac{[\mathrm{B}(X^n)]}{[\mathrm{B}(Y^l)]} = \frac{A(Y^l_k)\ I_f(X^n_m)}{A(X^n_m)\ I_f(Y^l_k)}$$

On account of similar constants among levels, the ratio of A factors reduces to

$$\frac{A(Y^l_k)}{A(X^n_m)} = \frac{[\langle X^0|X_0\rangle\langle Y^l|Y_k\rangle]^2\nu^3(Y^l_k)}{[\langle X^n|X_m\rangle\langle Y^0|Y_0\rangle]^2\nu^3(X^n_m)}$$

TABLE II: Calculated $A(i)/A(f)$ Factors (See Text)

state i	state f	$A(i)/A(f)$	state i	state f	$A(i)/A(f)$
0^0	30^1	1.02	0^0	17^1	1.04
0^0	8^1	1.24	30^1	30^2	1.08
0^0	30^2	1.06	30^1	8^1	1.21
0^0	30^3	1.10	8^1	8^130^1	1.02

The Franck–Condon factors above have been derived from the usual normal-mode expression that for pDFB with 30 modes is

$$FC(X_m^n) = [\langle 1^0|1_0\rangle\cdots\langle X^n|X_m\rangle\langle Y^0|Y_0\rangle\cdots\langle 30^0|30_0\rangle]^2$$

A listing of calculated A factor ratios is given in Table II where the transitions are always those given in Table I. The Franck–Condon factors have in every case been calculated with harmonic normal-mode wave functions. Earlier spectroscopic studies[14] have provided enough data for calculations with sufficient accuracy.

The Kinetic Model. The kinetic model developed for the earlier benzene study is applicable to pDFB with minor modifications. We will use a closely related nomenclature and retain the rate constant numbering scheme of that model.

B_0 represents unexcited S_0 pDFB, $B(0^0)$ is S_1 pDFB in the initially pumped S_1 pDFB level, and B(f) is S_1 pDFB in the final vibrational level f reached by collision energy transfer. Specific identification of that level is included in the nomenclature when necessary. We use B to represent the distribution of S_1 levels reached by collisional transfer.

$B(0^0)$ is prepared by absorption of UV radiation tuned to the maximum in the 0_0^0 absorption band.

$$B_0 + h\nu \rightarrow B(0^0)$$

$B(0^0)$ decays by radiative and nonradiative processes.

$$B(0^0) \xrightarrow{k_1} B + h\nu \quad (1)$$

$$B(0^0) \xrightarrow{k_2} \text{nonfluorescing states} \quad (2)$$

$B(0^0)$ can also decay by collisions with B_0 or foreign gas M that cause vibrational excitation into the S_1 field of levels B

$$B(0^0) + B_0 \xrightarrow{k_3} B + B_0 \quad (3)$$

$$B(0^0) + M \xrightarrow{k_4} B + M \quad (4)$$

Reactions 3 and 4 can be rewritten in terms of specific state-to-state processes.

$$B(0^0) + B_0 \xrightarrow{k_3(f)} B(f) + B_0 \quad (3a)$$

$$B(0^0) + M \xrightarrow{k_4(f)} B(f) + M \quad (4a)$$

k_3 and k_4 are the sums $\sum k_3(f)$ and $\sum k_4(f)$, respectively, taken over all S_1 levels B(f).

Each final state B(f) reached by vibrational energy transfer undergoes the same types of deactivation processes as $B(0^0)$.

$$B(f) \xrightarrow{k_1^*} B_0 + h\nu \quad (1^*)$$

$$B(f) \xrightarrow{k_2^*} \text{nonfluorescing states} \quad (2^*)$$

$$B(f) + B_0 \xrightarrow{k_3^*} B + B_0 \quad (3^*)$$

$$B(f) + M \xrightarrow{k_4^*} B + M \quad (4^*)$$

Quantitative measurements of band intensities can be made with pDFB pressures so low that collisional processes involving unexcited pDFB (B_0) do not compete measurably with the collision-free decay of S_1 pDFB levels. For example, it was frequently possible to use only 10^{-2} Torr of pDFB for the kinetics measurements. If we assume an approximately hard-sphere collisional rate constant $k_q \approx 10^7$ Torr^{-1} s^{-1} for B_0 acting on some state B, then the collisional decay rate of that state would be $k_q[B_0] \simeq (10^7 \text{ Torr}^{-1} \text{ s}^{-1})(10^{-2} \text{ Torr}) \approx 10^5 \text{ s}^{-1}$. When compared with the collision-free pDFB 0^0 decay rate $k_1 + k_2 \approx \tau_0^{-1} \approx 9 \times 10^7$ s^{-1} determined by direct collision-free fluorescence lifetime τ_0 measurements,[13] it is seen that collisional processes involving unexcited pDFB are noncompetitive. Even if the collisional rate constant were an order of magnitude larger or if B_0 pressures increased an order of magnitude (or both), these collisional processes would remain poor competitors with collision-free decay.

Processes by which added gases quench the S_1 electronic state have been omitted from the kinetic scheme. Experimental measurements of total fluorescence intensity in the region 25 500–36 000 cm^{-1} were made as Ar pressures increased from 0 to 3.1×10^4 Torr. The intensity at the highest added gas pressure was within 80% of the collision-free value. The collisional quenching rate constant is thus less than 10^4 Torr^{-1} s^{-1} so that quenching cannot compete with any measured VET processes. Quenching by He is expected to be at least as inefficient, given that the most probable quenching interaction with Ar is collision-induced intersystem crossing by heavy-atom enhancement of the spin–orbit matrix element.

While the present experiments used pulsed laser excitation, the gated fluorescence observation window of 50 ns exceeds $\tau_0 \approx 11$ ns sufficiently so that almost all of the S_1 fluorescence excited by each pulse is monitored. Under these conditions, a steady-state treatment of the kinetic scheme is valid.

The steady-state approximation gives the usual Stern–Volmer relationship for the intensity of the initially pumped 0^0 level as a function of added gas M. If $I_f^M(0^0)$ and $I_f^0(0^0)$ denote the observed 0^0 fluorescence intensity with and without added gas, respectively, then

$$\frac{I_f^0(0^0)}{I_f^M(0^0)} = 1 + \frac{k_4}{k_1 + k_2}[M] \quad (5)$$

The most useful relationship for deriving state-to-state rate constants $k_4(f)$ involves the population ratio

$$\frac{[B(0^0)]}{[B(f)]} = \frac{k_4^*}{k_4(f)} + \frac{k_1^* + k_2^*}{k_4(f)}\left(\frac{1}{[M]}\right) \quad (6)$$

The relationship $I_f(f) = A(f)\,B(f)$ transforms eq 6 into the intensity ratio

$$\frac{I_f(0^0)}{I_f(f)} = \left[\frac{[A(0^0)]}{[A(f)]}\right]\left[\frac{k_4^*}{k_4(f)} + \frac{k_1^* + k_2^*}{k_4(f)}\left(\frac{1}{[M]}\right)\right] \quad (7)$$

Measurements of k_4 and k_4^*. The rate constant k_4 for collisional VET from 0^0 into the entire field of S_1 levels can be obtained by monitoring the 0^0 intensity via the 5_1^0 band as collision partner pressures are increased. In a similar manner, k_4^* describing similar VET from a higher level can be measured in an analogous but separate experiment where the laser pumps the level directly.

The data in the form $I_f^0(0^0)/I_f^M(0^0)$ or $I_f^0(f)/I_f^M(f)$ are plotted in the Stern–Volmer form of eq 5. An example is shown in Figure 3 for both partners Ar and He. The constant k_4 is calculated from the slope of eq 5, using $(k_1 + k_2)^{-1} = \tau_0 = 11$ ns for most levels, a value taken or extrapolated from fluorescence lifetime measurements.[13]

Table III lists rate constants k_4 and k_4^* so measured. Each constant represents an average of at least three independent sets of data.

Measurement of the State-to-State Rate Constants $k_4(f)$. Our compendium of state-to-state rate constants from the 0^0 level is given in Table IV for Ar and He collisions. They are derived from fluorescence band intensities with the kinetic model introduced above.

The model is valid for any final level that is populated dominantly by the one-collision path $0^0 \rightarrow f$. This criterion is easily fulfilled for some VET channels by restricting measurements to low added gas pressures that yield only the very initial stages of VET.

pDFB proves to be a special case among the aromatics so far studied in that one type of VET channel has a rate constant exceeding that for any other by nearly an order of magnitude.

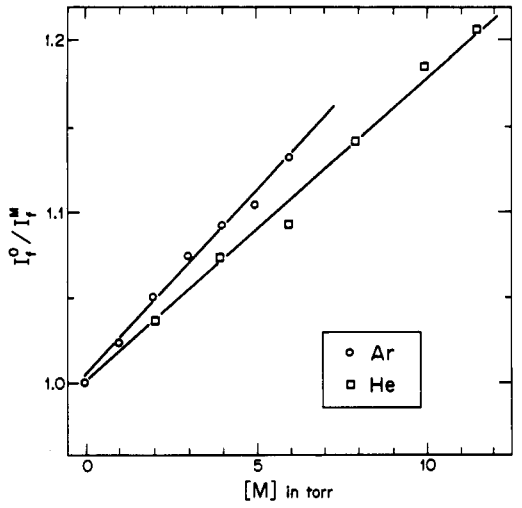

Figure 3. The intensity ratio I_f^0/I_f^M of the 5_1^0 fluorescence band plotted against the pressure of added Ar or He according to eq 5. I_f^0 and I_f^M are the intensities without and with added gas at pressure M, respectively.

TABLE III: Rate Constants k_4 for the 0^0 Level or k_4^* for Higher Levels Describing Vibrational Energy Transfer from That Level into the Entire Field of S_1 Levels

collision partner	level	k_4 or k_4^*, 10^6 Torr^{-1} s^{-1}
Ar	0^0	1.8 ± 0.2
	30^1	4.9 ± 0.4
	8^1	2.6 ± 0.2
	30^2	6.7 ± 0.3
	8^130^1	5.3 ± 0.5
	$[30^3]^a$	$[7.5 \pm 1.0]^a$
He	0^0	1.6 ± 0.2
	30^1	3.0 ± 0.3
	8^1	3.0 ± 0.3

[a] Estimated, not measured, as extrapolated from values for 0^0, 30^1, and 30^2.

TABLE IV: State-to-State Rate Constants, $k_4(f)$, for Vibrational Energy Transfer from 0^0 pDFB by Collisions with Ar and He

collision partner	final state	$k_4(f)$, 10^5 Torr^{-1} s^{-1} method A[a]	method B[b]	$k_4(f)^c/k_4^*$
Ar	30^1	16 ± 2	18 ± 2 (13)[d]	0.89
	8^1	2.8 ± 0.3	2.9 ± 0.4 (13)[d]	0.16
	30^2		1.7 ± 0.4 (12)[e]	0.09
	8^130^1		$0.1^{+0.1}_{-0.5}$ (2)[e]	0.01
	30^3		$0.5^{+0.5}_{-0.3}$ (4)[f]	0.03
He	30^1	9.5 ± 0.5	9.3 ± 0.5 (7)[d]	0.59
	8^1		4.3 ± 0.5 (2)[d]	0.27

[a] Calculated from the slope of eq 7. [b] Calculated for each intensity measurement. See footnotes *d*, *e*, and *f*. The number in parentheses indicates the number of intensity measurements over which the average was taken. [c] Denominator is k_4 or k_4^* as appropriate with values taken from Table III. [d] Calculated by eq 8. [e] Calculated by eq 9. [f] Calculated by eq 10.

The special channels occur when the only state change is $\Delta v_{30} = \pm 1$. These channels place challenges for quantitative measurements of some less efficient state-to-state transfers. We introduce below special treatments for them.

Single-Collision Channels: $0^0 \rightarrow 30^1$ and $0^0 \rightarrow 8^1$. We can be certain that the data providing the rate constants $k_4(30^1)$ and $k_4(8^1)$ are obtained under one-collision conditions. If we rather arbitrarily define the one-collision added gas pressure regime as that where the fraction of $B(0^0)$ decay occurring by the most favored VET channel is less than 0.1, we deduce from the largest observed rate constants [$k_4(30^1) \approx 2 \times 10^6$ Torr^{-1} s^{-1} for Ar and 9×10^5 Torr^{-1} s^{-1} for He (see below)] upper limits of 4.6 Torr for Ar and 10 Torr for He. Our quantitative measurements of the 30^1 and 8^1 growth band intensities were always made with added gas pressures at least an order of magnitude less.

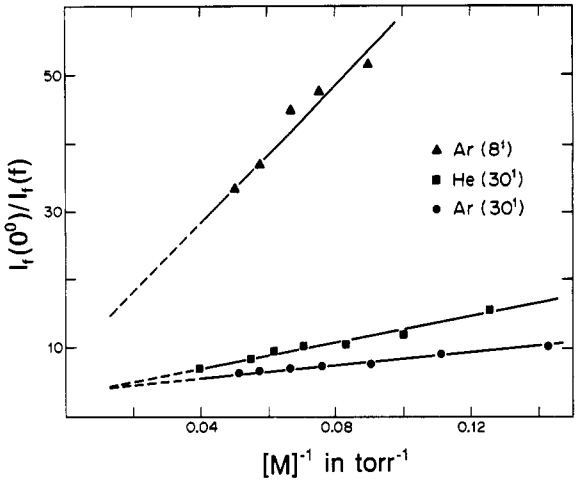

Figure 4. The intensity ratio $I_f(f)/I_f(0^0)$ plotted against the pressure [M] of added Ar or He in the form of eq 7. $I_f(f)$ is the intensity of the $5_1^08_1^1$ fluorescence band from the final state 8^1 or the $5_1^030_1^1$ band from the final state 30^1. $I_f(0^0)$ is the intensity of the 5_1^0 band.

Alternative averaging methods have been used to extract $k_4(f)$ values from measurements of the ratio $I_f(0^0)/I_f(f)$ as a function of added gas pressure M. In method A, the intensity ratios are plotted against 1/[M] in the form of eq 7. Examples of such plots are shown in Figure 4. The rate constant k_4 is extracted from the least-squares slope. The sum $k_1^* + k_2^* = 9.1 \times 10^7$ Torr^{-1} s^{-1} in eq 7 is taken from the collision-free fluorescence lifetime.[13] Each rate constant is an average of at least two independent sets of experiments.

Method B includes additionally the use of the intercept of eq 7. That equation is solved for $k_4(f)$ to obtain

$$k_4(f) = \frac{I_f(f)}{I_f(0^0)} \frac{A(0^0)}{A(f)} \left(k_4^* + \frac{k_1^* + k_2^*}{[M]} \right) \qquad (8)$$

With the values of k_4^* listed in Table III and the sum $(k_1^* + k_2^*)$ as above, $k_4(f)$ is calculated from eq 8 for each measurement of the intensity ratio observed at a given added gas pressure. The resulting set of $k_4(f)$ values is then averaged.

The entries in Table IV show that $k_4(f)$ values from the two methods agree to within their experimental error.

One- and Two-Collision Channels: $0^0 \rightarrow 30^2$ and $0^0 \rightarrow 8^130^1$. One can reach these final states by the one-collision processes above or alternatively by two-collision sequences

$$0 \rightarrow 30^1 \rightarrow 30^2$$

$$0 \rightarrow 30^1 \rightarrow 8^130^1$$

$$0 \rightarrow 8^1 \rightarrow 8^130^1$$

Since the sequences each involve a highly efficient $\Delta v_{30} = 1$ step, their competition with the relatively inefficient one-collision channels will occur relatively early as added gas pressures increase. Further, since these channels are all comparatively inefficient, quantitative measurement must involve added gas pressures somewhat above those of the previous section.

An expression for the final-state intensities can be developed from the kinetic model by including both one- and two-collision sequences.[28] For the $0^0 \rightarrow 30^2$ processes, convenient data analysis derives from the intensity ratio

$$\frac{I_f(30^2)}{I_f(30^1)} = \frac{A(30^2)}{A(30^1)} \left[\frac{k_4(30^1 \rightarrow 30^2)[M]}{c_2} + \frac{k_4(30^2)c_1}{k_4(30^1)c_2} \right] \qquad (9)$$

The constants c_1 and c_2 are the rate constant sums $(k_1^* + k_2^*)$ for the levels 30^1 and 30^2, respectively. Both are estimated to be 9.1×10^7 s^{-1} from fluorescence lifetime measurements.[13] The state-to-state rate constant $k_4(30^1 \rightarrow 30^2) = 1.6 \times 10^6$ Torr^{-1} s^{-1} as determined in an independent experiment.[28]

The first and second terms in brackets of eq 9 derive from the two-collision and one-collision paths, respectively. Given that

TABLE V: Rate Constant $k_4(30^2)$ Calculated from the Relative Intensity of Growth Bands from 30^2 and 30^1 When Ar Is the Collision Partner

[Ar], Torr	$I_f(30^2)/I_f(30^1)$	$k_4(30^2)$,[a] 10^5 Torr^{-1} s^{-1}
7.0	0.1678	1.6
9.0	0.1912	1.8
11.0	0.1942	1.7
13.0	0.2155	1.9
15.0	0.2053	1.6
17.0	0.2156	1.7
19.0	0.2193	1.6

[a] Calculated from eq 9. The average of values in the column is 1.7.

$k_4(30^2)$ turns out to be about 2×10^5 Torr^{-1} s^{-1} for Ar, one can see that the two-collision sequences makes a 10% contribution to the observed intensity ratios when added Ar pressure has increased to about 0.5 Torr.

Twelve measurements of the fluorescence intensity ratio were made with Ar pressures extending well beyond the 10% value. Equation 9 was solved for $k_4(30^2)$ for each ratio, and the resulting set of $k_4(30^2)$ values was averaged to yield the value given in Table V.

Table V contains a sample of the data chosen from those experiments with the higher Ar pressures. It is seen that as added gas pressures more than double, the $k_4(30^2)$ values so derived remain stable near 1.7×10^5 Torr^{-1} s^{-1}. Thus, eq 9 derived for the two-step sequence appears to be a reasonable representation of the data.

Energy transfer to the final state $8^1 30^1$ was treated in a similar manner with inclusion of the three paths given above. The rate constant $k_4(8^1 30^1)$ was calculated from an equation analogous to eq 9, using, as before, rate constants for intermediate steps that were measured in independent experiments.[28] The average value of $k_4(8^1 30^1)$ in Table IV comes from just two intensity measurements and is probably accurate only to within a factor of 2.

One-, Two-, and Three-Collision Channels: $0^0 \rightarrow 30^3$. The options for 30^3 population involve the four processes

$$0^0 \rightarrow 30^3$$

$$0^0 \rightarrow 30^1 \rightarrow 30^3$$

$$0^0 \rightarrow 30^2 \rightarrow 30^3$$

$$0^0 \rightarrow 30^1 \rightarrow 30^2 \rightarrow 30^3$$

Since we expect $0^0 \rightarrow 30^3$ to be inefficient, the two- and three-collision sequences may compete measurably at the necessary added gas pressures. The kinetic expressions for extraction of $k_4(30^3)$ includes all four processes to give the ratio

$$\frac{I_f(30^3)}{I_f(30^1)} = \frac{A(30^3)}{A(30^1)}\left\{\frac{c_1 k_4(30^3)}{c_3 k_4(30^1)} + \frac{k_4(30^1 \rightarrow 30^3)[\mathrm{M}]}{c_3} + \frac{c_1 k_4(30^2) k_4(30^2 \rightarrow 30^3)[\mathrm{M}]}{c_2 c_3 k_4(30^1)} + \frac{k_4(30^1 \rightarrow 30^2) k_4(30^2 \rightarrow 30^3)[\mathrm{M}]^2}{c_1 c_2}\right\} \quad (10)$$

The terms in brackets successively derive from the four sequences given above. The intermediate-step rate constants such as $k_4(30^1 \rightarrow 30^3)$ can all be obtained in independent experiments,[28] and those values are used in the determination of $k_4(30^3)$. The constants c_1, c_2, and c_3 are the sums $(k_1^* + k_2^*)$ for the states 30^1, 30^2, and 30^3, and in each case the sum is approximated by 9.1×10^7 s^{-1} derived from fluorescence lifetime measurements.[13] The $k_4(30^3)$ value reported in Table IV is the average of four values calculated from eq 10 from four different Ar pressures. Given the complexity of eq 10 and the uncertainties in the many rate constants needed to obtain $k_4(0^0 \rightarrow 30^3)$, the value in Table IV can be considered accurate to within only about a factor of 2.

A calculation with approximate rate constants shows that the sequential processes together begin to contribute at least 10% to the fluorescence intensity ratio when the added Ar pressure has risen to about 1 Torr.

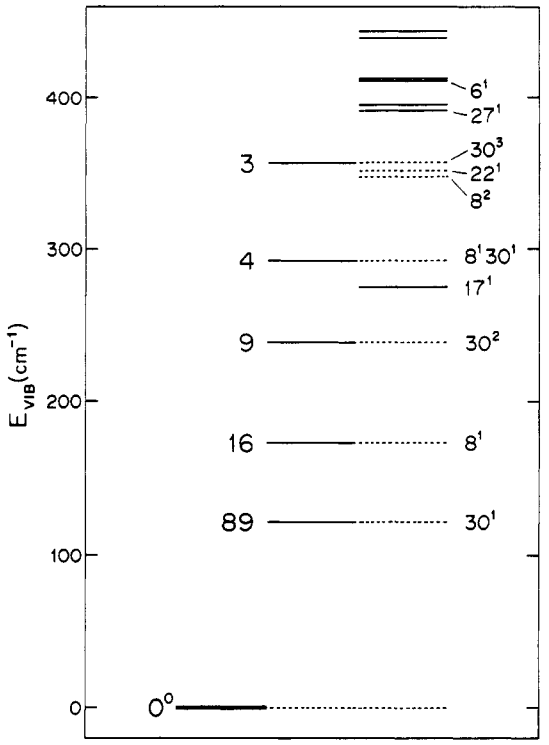

Figure 5. A schematic diagram of all of the vibrational levels in S_1 pDFB up to 450 cm^{-1}. The vibrational identity is given for most levels at the right. The most efficient channels for vibrational excitation are indicated by the levels pulled out of the stack. The number at the left of these levels is the percent of total VET occurring in that channel (i.e., $k_4(f)/k_4$ multiplied by 100).

Discussion

These experiments have characterized the vibrational energy flow from the 0^0 level of S_1 pDFB during 300 K collisions with Ar and with He. The results are summarized in Tables III and IV. Table III shows the measured absolute rate constant, k_4, for destruction of the 0^0 level by VET into the entire field of S_1 levels. It also contains the analogous constants k_4^* for higher initial S_1 levels. Table IV lists the state-to-state rate constants $k_4(f)$ for one-collision transfers from 0^0 to the final states f.

If the experiments have succeeded in monitoring every state-to-state transfer from a given initial level, then we should observe that $\sum k_4(f) = k_4$, at least to within the uncertainty of the measured rate constants. The observed ratio $\sum k_4(f)/k_4$ for Ar collisions is 1.17, exceeding unity because of experimental uncertainties.

The earlier studies of VET in S_1 aromatics have produced general behavior patterns with two prominent characteristics. First, the VET is highly selective among a choice of accessible final levels. Second, the competition between VET channels from a given initial level is almost identical for a wide variety of collision partners. The pDFB data are consistent with the first characteristic but not with the second.

Consider first the final-state selectivity. When it is seen that 13 S_1 levels lie within about $2kT$ of 0^0, or that almost 40 are within $3kT$, or that more than 110 levels lie within $4kT$, the extraordinary pDFB selectivity can be placed in proper perspective. Table IV shows that just three of those possible channels account for almost all of the VET with Ar collisions. Further, the $0^0 \rightarrow 30^1$ channel alone has almost 90% of the VET. The state-to-state processes with He collisions are similarly selective. The two measured channels have nearly 90% of the VET.

The state-to-state vibrational energy-transfer data are most clearly displayed by flow patterns that describe the percent of energy flow from the pumped level into each nearby level. The flow pattern for Ar is given in Figure 5 where every level to about

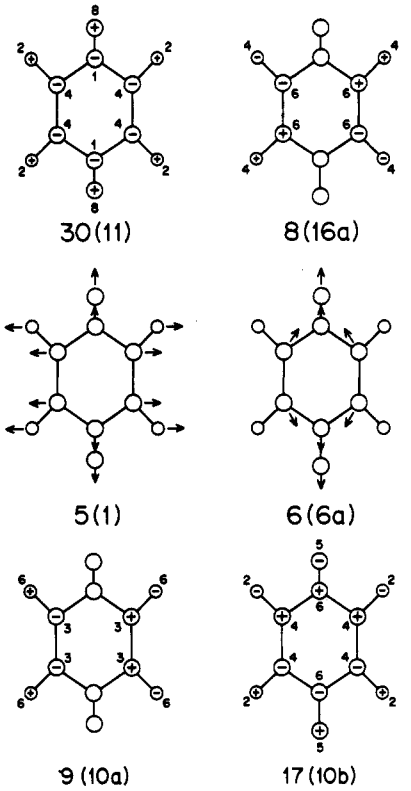

Figure 6. Some normal modes for pDFB. The numbers that appear on the out-of-plane modes are relative atomic displacements calculated by Schmid (Schmid, E. W. *Z. Electrochem.* **1960**, *64*, 940).

450 cm^{-1} above the 0^0 level is included. In this representation, the selectivity becomes even more apparent. For example, transfer to the level $8^1 30^1$ is large enough to be measured while flow to a lower energy fundamental, 17^1, is too small to be measured. Alternatively, the three-quantum transition to 30^3 with Ar collisions is measurable while transfer to the fundamental 27^1, lying at about the same energy, cannot be observed. As we show elsewhere,[28] the selectivity of collisional vibrational energy flow from higher S_1 levels is even more extreme.

Figure 5 also shows that $\nu_{30} = 119$ cm^{-1} is the most active mode. The display in Figure 6 shows that ν_{30}, the lowest frequency S_1 energy mode in pDFB, is an out-of-plane mode. As such, conventional experience with VET would predict its dominant activity. Indeed, these characteristics have been suggested[21] as the reason why ν_{30} is the only participant in S_0 energy flow as seen in crossed-beam scattering from He. We will return to this point later.

With He collisions, the $0^0 \rightarrow 8^1$ channel is far more competitive with the dominant $0^0 \rightarrow 30^1$ channel than is the case for Ar collisions. This behavior was a surprise since an accumulation of experience beginning with the original benzene study consistently showed similar VET patterns for different collision partners. The resolution of the enigmatic pDFB results is an interesting story that emerges from the discussion of the SSH-T model below.

1. Quantal Scattering Theory. Modern theoretical treatment of state-to-state VET in large polyatomics began with Clary's treatment of systems for which experimental data are sparse (He + C_2H_4)[36] or still nonexistent (He + cyclopropane).[37] The approach has since been extended to other polyatomics to take advantage of experimental cross sections. The He + pDFB system is among them.[27]

The three-dimensional scattering theory approach uses vibrational close coupling (VCC) with the rotational infinite-order sudden approximation (IOS). Clary has given a general discussion of the theory and a review of some applications.[31] Another review has been given from the experimentalist's point of view.[7]

Most of the pDFB + He calculations are tailored specifically to vibrationally inelastic scattering in the S_0 state to take advantage of experimental crossed beam cross sections. Those experiments involve vibrational excitation from rotationally cold 0_0 molecules as a function of the He center-of-mass collision energy, $E_{c.m.}$. Only two channels occur, $0_0 \rightarrow 30_1$ and $0_0 \rightarrow 30_2$. Both are monitored as a function of $E_{c.m.}$ dependence, and they further show that the one-quantum channel $0_0 \rightarrow 30_1$ dominates the scattering. Six S_0 modes have frequencies below about 450 cm^{-1}. The calculated cross section for reaching the lowest mode $\nu_{30}'' = 157$ cm^{-1} exceeds the other single-mode cross sections by an order of magnitude.

The S_1 calculations explored only the two largest experimental channels for He collisions, $0^0 \rightarrow 30^1$ and $0^0 \rightarrow 8^1$. The calculated constants for 300 K collisions show good agreement with our Table IV values. The calculated ratio of the two calculated rate constants is 1.7. The observed ratio is 2.2. The most severe test concerns absolute values, and here the agreement is even more impressive. The comparisons of calculated and experimental rate constants set forth in Clary's Table VI show agreement to within a factor of 2, the calculated values being overestimates. In contrast, the old SSH-T prescriptions would have underestimated absolute values by orders of magnitude.

It should be remarked that these large-scale VCC-IOS calculations were made with very approximate interaction potentials. The satisfying agreement of these and other calculations with experiments is encouraging since it suggests that fine details of the potentials may not generally prove crucial to success.

2. The SSH-T Model. The standard treatment of collision-induced energy transfer in polyatomic molecules is based on adaptations of Schwartz, Slawsky, and Herzfeld's (SSH)[29,38] quantum mechanical scattering treatment of atom–diatom collisions. The principal adaptation to polyatomic molecules is due to Tanczos,[30] hence the acronym SSH-T. Aspects of the theories are described in various monographs and reviews.[39-43]

For S_1 aromatic studies, the SSH-T approach has been used by various authors to develop propensity rules for the competition among possible VET channels. The basic relationship for the relative magnitude of a state-to-state channel in which, say, two modes ν_a and ν_b undergo quantum changes between the initial and final states is

$$P_{if}(\Delta v_a, \Delta v_b) \propto C_{if} I(\Delta E) V_a^2 V_b^2 \qquad (11)$$

Here the probability, P_{if}, of a specific state-to-state process involving the normal modes ν_a and ν_b is a product of three factors. The V^2 terms are vibrational matrix elements appearing independently for each normal mode undergoing a quantum change. The term $I(\Delta E)$ is primarily dependent upon the amount of energy, ΔE, that is exchanged V $\leftrightarrow$ T during the transfer. The term C_{if} is a correction term to the SSH-T model introduced by McDonald and Rice[12] reminiscent of the steric factors used by Tanczos.[30] The C_{if} term accounts explicitly for the coupling of vibrational motions with the collisional trajectories.

In the sections below, we develop expressions for each factor in eq 11, tailored for our pDFB collisional systems. The pDFB treatments will be seen to be only modest modifications of those developed for other aromatics, beginning with the original benzene experiments.[5] The end result is a set of propensity rules in the form of eq 11 that describe semiquantitatively the competition

(36) (a) Clary, D. C. *J. Chem. Phys.* **1984**, *81*, 4466; (b) *Mol. Phys.* **1984**, *51*, 1299.
(37) Clary, D. C. *J. Am. Chem. Soc.* **1984**, *106*, 970.
(38) The theory was developed independently by K. Takayanagi. For an excellent historical discussion and assessments of the theory see the review: Takayanagi, K. *Prog. Theor. Phys. Suppl.* **1963**, *25*, 1.
(39) Ormonde, S. *Rev. Mod. Phys.* **1975**, *47*, 193.
(40) Lambert, J. D. *Vibrational and Rotational Relaxation in Gases*; Clarendon Press: Oxford, 1977.
(41) Stretton, J. L. *Transfer and Storage of Energy by Molecules*; Burnett, G. M., North, N. M., Eds.; Wiley-Interscience: New York, 1969; Vol. 2, Chapters 1 and 2.
(42) Yardley, J. T. *Introduction to Molecular Energy Transfer*; Academic Press: New York, 1980.
(43) Cottrell, T. L.; McCoubrey, J. C. *Molecular Transfer in Gases*; Butterworths: London, 1961; p 141.

TABLE VI: Collisional Coupling Terms C_{if} for $\Delta v = 1$ Changes in the Normal Modes of pDFB

mode[a]	C_{if}	nature
1 (2)	0.00	in-plane
2 (8a)	0.00	in-plane
3 (7a)	0.00	in-plane
4 (9a)	0.00	in-plane
5 (1)	0.00	in-plane
6 (6a)	0.085	in-plane
7 (17a)	0.015	out-of-plane
8 (16a)	0.20	out-of-plane
9 (10a)	0.023	out-of-plane
10 (20a)	0.00	in-plane
11 (19a)	0.00	in-plane
12 (13)	0.00	in-plane
13 (18a)	0.00	in-plane
14 (12)	0.00	in-plane
15 (5)	0.08	out-of-plane
16 (4)	0.15	out-of-plane
17 (10b)	0.047	out-of-plane
18 (20b)	0.00	in-plane
19 (19b)	0.00	in-plane
20 (14)	0.00	in-plane
21 (18b)	0.00	in-plane
22 (15)	0.00	in-plane
23 (7b)	0.00	in-plane
24 (8b)	0.00	in-plane
25 (3)	0.00	in-plane
26 (6b)	0.085	in-plane
27 (9b)	0.00	in-plane
28 (17b)	0.010	out-of-plane
29 (16b)	0.10	out-of-plane
30 (11)	0.20	out-of-plane

[a] Wilson's numbering (Wilson, Jr., E. B. *Phys. Rev.* **1934**, *45*, 706). Herzberg's numbering is in parentheses (Herzberg, G. *Infrared and Raman Spectra*; Van Nostrand: Princeton, NJ, 1945; p 118).

among state-to-state 0^0 VET channels. Elsewhere we have used the rules with similar success to account for VET from higher S_1 pDFB levels.[28]

The Collisional Factor, C_{if}. These factors were derived from the recipes of McDonald and Rice[12] for their treatment of benzene. The details of the calculations are given in the Appendix. Table VI lists the C_{if} factors for $\Delta v = 1$ changes in each normal mode along with identification of in-plane or out-of-plane character. Note that many of these factors are zero (particularly for most of the in-plane modes), and once a molecule begins to vibrate in one of those normal modes, that mode cannot collisionally change quantum number according to the model. This extreme assumption does not affect the modeling of the present data (see below).

We introduce a modification to the treatment of McDonald and Rice[12] involving multiple-quantum changes in a mode. If C_{if} is truly a steric factor, then multiple-quantum changes in the same mode should be weighted with the same factor as $\Delta v = 1$ changes in that same mode. We adopt this rule. We have left the Δv discrimination for the vibrational matrix elements, V^2, to be discussed shortly.

The $I(\Delta E)$ Factor. The original SSH-T presentation[29] derived this factor using the intermolecular potential

$$V(r) = \exp[-\alpha^* r] - \epsilon \qquad (12)$$

where r is the intermolecular distance, α^* is the steepness parameter (in Å^{-1}) that, by various methods, fits the potential at the repulsive wall at an energy of maximum transfer probability, and ϵ is the intermolecular well depth.

Stretton[41,44] and also Lambert[45] have discussed the problems of establishing α^*. They have listed the α^* values determined for a number of systems at various temperatures. The values invariably lie in the range 4–5.5 Å^{-1}. Thus, the parameter should be narrowly defined for the pDFB experiments.

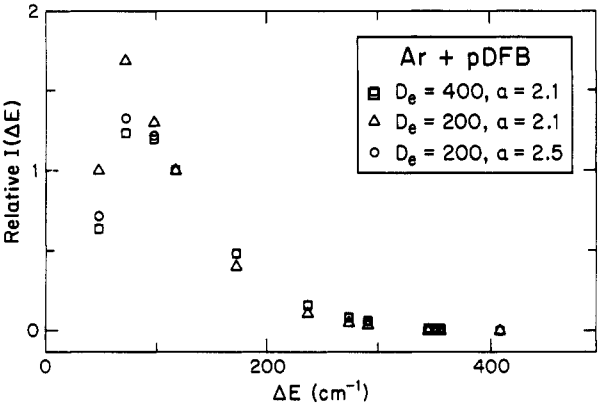

Figure 7. $I(\Delta E)$ calculated by numerical integration plotted against ΔE for various combinations of D_e (cm^{-1}) and a (Å^{-1}) associated with Ar + pDFB collisions. The three plots are normalized to unity at ΔE = 120 cm^{-1}.

Plots of $I(\Delta E)$ made by numerical integration of Tanczos' formula and are summarized in Figure 7 of ref 5. They are calculations made by others on three 300 K systems: CH_3Cl, CH_3F, and CH_4. All have reasonably similar $I(\Delta E)$ plots. The similarity occurs because the two parameters most important in establishing $I(\Delta E)$, namely α^* and the reduced mass, do not vary greatly among the systems.

An analytical expression for the $I(\Delta E)$ integral with the potential of eq 12 is available[30] for the limit of high temperatures or large ΔE. While we do not use it here, it is important because McDonald and Rice[12] have used extensively a variant in their discussion of the flow patterns in aniline, pyrazine, and benzene. Their analytical expression is identical with that of Tanczos[30] except that they replaced a preexponential $|\Delta E|^{7/3}$ dependence with $|\Delta E|^{4/3}$. The latter occurs for a form of the SSH model by Cottrell and McCoubry[43] that combines the vibrational matrix elements with the ΔE dependence. The 4/3 dependence is not strictly appropriate for treatments such as SSH-T that separate completely these factors.

$I(\Delta E)$ has also been derived for more realistic potentials containing an attractive well. The use of such potentials should be particularly important for the present study where some VET transitions involve ΔE values that are on the same order as the Ar–pDFB well depth. Shin[46] has provided analytical forms for $I(\Delta E)$ for a Morse potential and also a Lennard-Jones potential. Unfortunately, they are appropriate only for ΔE values larger than those in our experiments.

Alternatively, one can evaluate $I(\Delta E)$ numerically. We use a numerical integration of Thompson's formula for a Morse potential.[47]

All $I(\Delta E)$ functions have primary dependence on ΔE, T, μ, and the constants of the potential. They all can be evaluated for pDFB–Ar. In the case of a Morse potential

$$V(x) = \epsilon(e^{-2ax} - 2e^{-ax}) \qquad (13)$$

where x is the displacement from the potential minimum, and the potential constants are a and ϵ. The a parameter is related to the α^* parameter of SSH-T by the approximation $2a \approx \alpha^*$. Thus, we expect a to be in the range 2–2.5 Å^{-1}, according to Stretton's analysis.[44] We know from study of the pDFB–Ar van der Waals complex[23] that $\epsilon \approx 200$ cm^{-1}.

We show in Figure 7 some calculations of $I(\Delta E)$ for pDFB + Ar using numerical integration with the Morse potential. Those $I(\Delta E)$ functions contain a Boltzmann factor since they pertain to T → V processes. The function for V → T processes would differ by the absence of this factor. The figure shows the sensitivity of $I(\Delta E)$ to the steepness parameter $\alpha \approx 2a$ and to the well depth ϵ. The curves represent combinations of the values a = 2.1 and 2.5 Å^{-1} with ϵ = 200 and 400 cm^{-1}.

(44) Stretton, J. L. *Trans. Faraday Soc.* **1965**, *61*, 1053.
(45) See pp 46–47 of ref 40.
(46) Shin, H. K. *J. Chem. Phys.* **1965**, *42*, 19.
(47) Thompson, S. L. *J. Chem. Phys.* **1968**, *49*, 3400.

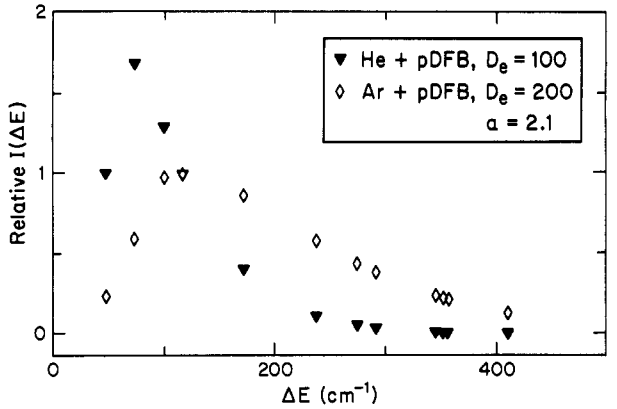

Figure 8. $I(\Delta E)$ calculated by numerical integration plotted against ΔE for He + pDFB and Ar + pDFB systems. Both use a = 2.1 Å^{-1}. The plots are normalized to unity at ΔE = 120 cm^{-1}. The D_e values are in cm^{-1}.

The basic message is that $I(\Delta E)$ is not very sensitive to these variations in the well depth or in the a value. There is obviously no justification in fine tuning $I(\Delta E)$ with these parameters. Thus, the $I(\Delta E)$ factor is essentially fixed in the form of Figure 7.

If we turn to the He + pDFB system, we see that $I(\Delta E)$ for a Morse potential (numerically integrated) is qualitatively different from that for Ar, primarily because of the difference in reduced mass. We compare the two cases in Figure 8, where a = 2.1 for both and the well depths are taken as 200 and 100 cm^{-1} for Ar[23] and He,[48] respectively. The big difference is the falloff at higher ΔE. It is steep above 100 cm^{-1} for Ar and relatively shallow for He. Thus, the $I(\Delta E)$ factor should make these collision partners behave quite differently. Large ΔE transitions should remain much more competitive with smaller ones in He + pDFB collisions.

The Vibrational Matrix Element V^2. The calculation of V_a^2 and V_b^2 for transfer in which modes ν_a and ν_b undergo quantum changes has been discussed by Stretton.[44,49] All modes are treated as independent normal-mode harmonic oscillators with the matrix element between the initial and final states being of the standard form. The interaction potential $V(r,Q)$ is purely repulsive

$$V(r,Q) \propto \exp[\alpha^*(-r - A_aQ_a - A_bQ_b - ...)] \qquad (14)$$

where Q_a, Q_b, ... are the normal coordinates and A_a, A_b, ... are the displacements of atoms along a normal coordinate per unit change in Q. Since the potential is separable in Q's, each vibrational quantum change represented by V_a^2, V_b^2, ... is independent of any other. Expansions of $V(r,Q)$ in a McLaurin series for, say, the term involving Q_a yields

$$V(Q_a) \propto 1 - \alpha^*A_aQ_a + (\alpha^*A_aQ_a)^2/2 - ... \qquad (15)$$

giving matrix elements of the familiar form $\langle\phi_i(a)|Q_a^n|\phi_f(a)\rangle$ for $\Delta v = n$. Evaluation[40] gives

$$\Delta v = 0 \qquad V_a^2 = 1$$

$$\Delta v = 1 \qquad V_a^2 = \frac{(\alpha^*A_a)^2(v_i + 1)}{2\gamma}$$

$$\Delta v = 2 \qquad V_a^2 = \frac{(\alpha^*A_a)^4(v_i + 1)(v_i + 2)}{16\gamma^2}$$

and so forth, where $\gamma = 4\pi^2\nu/h$. For transitions with $\Delta v = n$ from the 0^0 level where $v_i = 0$, the equations reduce to the compact form

$$V_a^2 = \frac{1}{|\Delta v|!}\left[\frac{(\alpha^*A_a)^2h}{8\pi^2\nu_a}\right]^{|\Delta v|} \qquad (16)$$

(48) Clary (ref 27) has obtained by calculation an (S_0) well depth of 186 cm^{-1} for He–pDFB, said by him to be very probably too deep. Experiments with van der Waals complexes show that there is little difference between the S_1 and S_0 well depths. (Su, M. C., private communication.)

(49) See p 79 of ref 41.

TABLE VII: Vibrational Matrix Elements, V_a^2, in the SSH-T Model for Selected Normal Modes of pDFB[a]

mode	fundamental frequency, cm^{-1}	V_a^2 Δv = 1	Δv = 2	Δv = 3
30	119	1.93	1.87	1.20
8	173	1.33	0.88	0.39
17	275	0.84	0.35	0.10
3	1251	0.18	0.017	0.0010

[a] Calculated by eq 41 with β = 230 cm^{-1}.

These matrix elements show that the falloff in transition probability with increasing Δv is highly sensitive to the values of α^*, A_a, and ν_a. In turn, the comparative values of V_a^2 and V_b^2 for a given Δv are primarily governed by $1/\nu$ since it, among all parameters, generally has the largest sensitivity to vibrational mode.

In principle, we can approximately evaluate V_a^2. As discussed before, the steepness parameter α^* varies little among collision pairs and ν_a is of course known. A_a^2 values for many polyatomic molecules are known by calculation to lie in the limited range 0.01–0.1 amu^{-1} for non-hydrogenic vibrations.[45] A_a^2 values could be derived for pDFB, but even so the Procrustean act of fitting pDFB to a breathing sphere model would render them of dubious value.

We have taken an alternative and empirical approach to the evaluation of the matrix elements. An equivalent form is

$$V_a^2 = \frac{1}{|\Delta v|!}(\beta/\nu_a)^{|\Delta v|} \qquad (17)$$

This form allows V_a^2 to be described by a single parameter β that is determined by fitting selected energy-transfer data. In this treatment we ignore the modest sensitivity that β should have to mode identity (due to A_a). A value of β, uniform among all modes, is derived in the following section.

The SSH-T Propensity Rules for pDFB. We are attempting to reproduce the observed flow patterns in the collisions of pDFB with Ar when the 0^0 level is pumped. Those patterns are summarized in Table IV and Figure 5. Since flow patterns are branching ratios among various final states, we will be concerned with the competition among final states or relative transition probabilities rather than absolute values.

Our use of SSH-T now focuses on evaluating P_{if} for each final state $|f\rangle$. P_{if} is the product of the three factors C_{if}, V_a^2, and $I(\Delta E)$ according to eq 11. $I(\Delta E)$ is taken directly from the numerically integrated $I(\Delta E)$ values displayed in Figure 8. The C_{if} factor is taken from Table VI. The V^2 factors require further discussion.

The factor V_a^2 occurs separately for each mode undergoing a quantum change. We use V_a^2 according to eq 17, where the constant β must be chosen. *This constant is the only adjustable parameter in our use of the SSH-T model.* With C_{if} and $I(\Delta E)$ chosen as above without recourse to energy-transfer data, we then choose β in order to reproduce the observed ratio of two secure energy-transfer rates, namely, $0^0 \rightarrow 30^1$ and $0^0 \rightarrow 30^2$.

Via the SSH-T model the ratio is

$$\frac{k_f(30^1)}{k_4(30^2)} = 9.4 = \frac{C_{if}(30)\ I(+119\ \text{cm}^{-1})\ V^2(30, \Delta v = +1, \nu = 119\ \text{cm}^{-1})}{C_{if}(30)\ I(+238\ \text{cm}^{-1})\ V^2(30, \Delta v = +2, \nu = 119\ \text{cm}^{-1})}$$

The C_{if} factors cancel. To replicate the experimental ratio 9.4, we find that β = 230 cm^{-1}. This empirical evaluation gives via eq 17 with β = 230 cm^{-1} an expression for V_a^2 that is valid for calculating relative P_{ij} among various channels for any given collision partner.

As an aside, it is interesting to see how these "experimental" V_a^2 matrix elements respond to increasing Δv for a few pDFB modes. The matrix elements for a few low-frequency modes Δv = 1, 2, and 3 are shown in Table VII. We also include a 1200-cm^{-1} mode to illustrate the behavior of the matrix elements with a

TABLE VIII: A Comparison of the Predictions of SSH-T Propensity Rules to Experimental Data

				pDFB + Ar				pDFB + He			
level	ΔE, cm^{-1}	$V^{2\,a}$	$C_{if}{}^b$	$I(\Delta E)^c$	$P(f)^d$	$k(f)^d$ (calc)	$k_4(f)^e$ (exptl)	$I(\Delta E)^g$	$P(f)^d$	$k(f)^d$ (calc)	$k_4(f)^e$ (exptl)
30^1	119	1.92	0.20	[100]	38.4	[16.0]	16	[100]	38.4	[9.5]	9.5
8^1	173	1.32	0.20	39.9	10.5	4.4	2.8	82.4	21.8	5.4	4.3
30^2	238	1.83	0.20	11.1	4.1	1.7	1.7	57.0	20.8	5.1	
17^1	275	0.83	0.047	5.2	0.20	0.08		44.3	1.7	0.43	
8^130^1	292	2.53	0.018	3.6	0.16	0.07	0.1	39.1	1.8	0.44	
8^2	346	0.87	0.20	1.2	0.21	0.09		25.5	4.4	1.1	
22^1	353	0.65	0.00	1.0	0.00	0.00		24.2	0.00	0.00	
30^3	357	1.18	0.20	0.92	0.22	0.09	0.5	23.3	5.5	1.4	
27^1	391	0.58	0.00	0.45	0.000	0.00		17.1	0.00	0.00	
17^130^1	394	1.59	0.0056	0.42	0.004	0.002		17.0	0.15	0.0328	
6^1	410	0.56	0.085	0.3	0.014	0.006		14.8	0.70	0.17	
8^130^2	411	2.41	0.018	0.3	0.013	0.005		14.6	0.63	0.16	

[a] Calculated by eq 41 with $\beta = 230$ cm^{-1}. [b] Given in eq 31. [c] Numerically integrated $I(\Delta E)$ for Ar + pDFB, normalized to a value of 100 for $\Delta E = 119$ cm^{-1}. [d] Calculated $k(f)$ is $P(f) = I(\Delta E)C_{if}V^2$ normalized to the experimental value of $k_4(0^0 \rightarrow 30^1)$. [e] Experimental rate constant in 10^5 Torr^{-1} s^{-1}. [f] As in footnote c, but with $I(\Delta E)$ for He + pDFB.

frequency more typical of a small S_0 molecule.

It is seen from Table VII that the matrix elements for the lower frequency modes fall off rather slowly with increasing Δv. It is also seen that $V_a{}^2$ for $\Delta v = 1$ channels falls off only slowly with increasing frequency of the mode. Thus, the mode discrimination among single-quantum changes for a heavy collision partner such as Ar occurs primarily on account of the $I(\Delta E)$ prohibition.

3. SSH-T Predictions for Ar + pDFB(0^0). Using eq 17 as described above, we calculate P_{ij} for each observed VET channel. The results are presented in Table VIII, where the set of P_{if} values has been normalized to a value of 16×10^5 Torr^{-1} s^{-1} for the $0^0 \rightarrow 30^1$ channel and listed as $k_4(f)$ (calc). This procedure allows easy comparison with the set of experimental $k_4(f)$ values.

An alternative comparison with the data is provided by using P_{if} to obtain a calculated ratio $k_4(f)/k_4$ describing the fraction of total VET that occurs via the channel (f).

To obtain a calculated $k_4(f)/k_4$, it is necessary to calculate an accurate replica of k_4 via the SSH-T rules. To do this, we calculate $k_4(f)$ values for every S_1 level up to some vibrational energy and take their sum as the relative calculated value of k_4. We have summed $k_4(f)$ for levels up to 2000 cm^{-1} with a computer-generated listing of all levels for which $\sum v_i \leq 8$. It was found that calculated values of $k_4(f)$ from levels above 500 cm^{-1} did not contribute significantly to the sum. The steep falloff in $I(\Delta E)$ and the prohibition imposed by multiple quantum changes damps out $k_4(f)$ for higher levels.

The comparisons with experimental data are given in Table VIII. Perhaps a more convenient comparison is shown in Figure 9 where we see only the blunt aspects of the data, namely, only those final states with the largest transfer rate constants. An assessment of the success of the SSH-T rules in modeling the transfer rates depends on one's prior expectations. Note, however, some aspects of the comparisons. We first see that the SSH-T predictions place essentially all of the transfer into those few (five) final states, consistent with the observation. The SSH-T calculations also replicate the data by confining the bulk of the transfer to the final states 30^1, 30^2, and 8^1, which in this case happen to be the three states with the lowest ΔE. The rules further agree with the data by placing relatively small probabilities on transfers to states above the lowest three. On the other hand, while the rules are forced by our fitting procedure to replicate the ratio of the $0^0 \rightarrow 30^1$ and $0^0 \rightarrow 30^2$ rates, they do not scale them quite correctly, particularly 30^1, with respect to the total energy transfer.

4. SSH-T Predictions for He + pDFB(0^0). Prior studies of vibrational energy flow in S_1 polyatomic molecules have revealed that flow patterns are not particularly sensitive to the identity of the collision partner. This insensitivity occurs within the proviso that we compare only those collision partners for which the principal channel for vibrational excitation/relaxation is V ↔ T. When large vibrationally complex polyatomic collision partners are used, the flow patterns are quite different due to the participation of V ↔ V resonances. A study of near-resonant OCS–benzene[50] transfer showed particularly how effective such V ↔ V transfer could be.

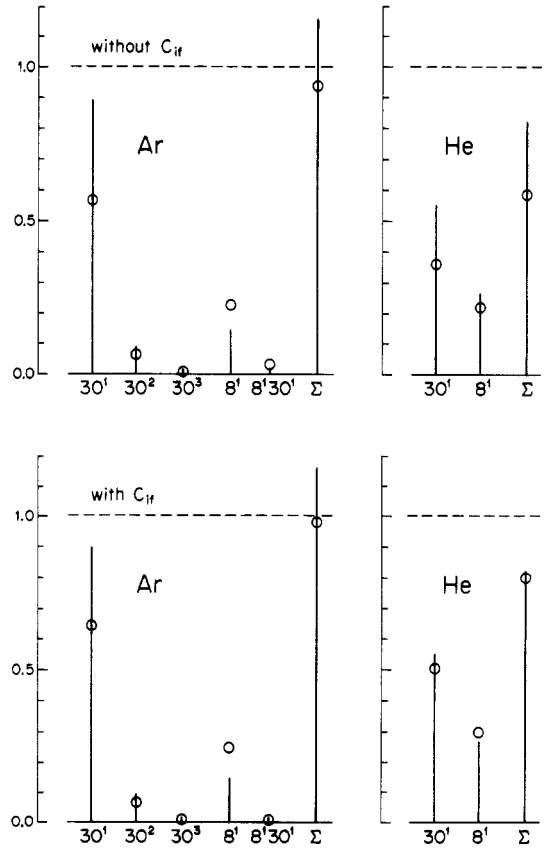

Figure 9. A display of the fractions of energy transfer from pDFB(0^0) that occur by specific state-to-state channels as given by the ratio of rate constants $k_4(f)/k_4$. The $\sum$ entry is the sum of the displayed fractions. $\sum$ would be in principle unity if VET from 0^0 occurred only by the displayed state-to-state channels. The bars are experimental values. The circles are values calculated from the SSH-T propensity rules. Both the experimental and calculated values for the Ar 30^3 and 8^130^1 channels are too small to show accurately. The two sets show the propensity rule calculations with and without the inclusion of the factor C_{if}.

The most impressive demonstration of the insensitivity of the V ↔ T flow patterns has been provided by Struve and co-workers[10] in a study of flow from 0^0 (S_1) aniline. That collisional transfer shows a remarkably uniform flow pattern among eight collision partners. This insensitivity to collision partner has, in fact, been incorporated into an alternative model for collision-induced vi-

(50) Atkinson, G. H.; Parmenter, C. S.; Tang, K. *J. Chem. Phys.* **1979**, *71*, 68.

brational energy flow in polyatomic molecules by Freed.[51]

In the face of the impressive documentation and past discussions of uniform flow patterns, it is a surprise in the present work that the experimental flow patterns for pDFB collisions with Ar and with He are markedly different. The display in Figure 9 shows that while the two principal final states remain the same, the relative rates into these states are quantitatively different. The experimental ratio $k_4(30^1)/k_4(8^1)$ is 2.2 for He collisions and 5.6 for Ar collisions.

More qualitative comparisons of the transfer with the two gases reveal further differences in behavior. Figure 1 show the fluorescence spectra in the region where growth bands occur due to energy transfer via the channels $0^0 \rightarrow 30^n$ (n = 1, 2, 3). The added gas pressures have been adjusted so that the destruction of the 0^0 state by collisions occurs to an equivalent extent (22% of the 0^0 state decay in each case). With the relative intensities of the spectra normalized to that of a 30^1 growth band, the contrasts are immediately apparent. The relative intensities of 30^2 and 30^3 bands differ substantially for the two gases. Transfer to 17^1 (E_{vib} = 275 cm^{-1}) is easily observed with the He collisions but not with the Ar collisions. Further, a new growth band, frustratingly unidentifiable by us, appears with the He collisions. Additionally, the band contours of the growth bands are different for He collisions than for Ar collisions. Those for the He collisions are much broader than those for the Ar collisions.

The SSH-T model with parameters appropriate for He shows why such different VET behavior ensues. It also reveals why other V ↔ T collision partners produce such uniform energy flow patterns. Examine in turn each of the three factors C_{if}, V_a^2, and $I(\Delta E)$ in eq 11 for sensitivity to collision partner. The C_{if} factors are completely independent of the identity of the collision partner. The factor V_a^2 contains only one parameter that is in principle collision partner dependent, namely α^*. As Stretton has discussed,[44] however, little variation should occur between values appropriate for He and Ar. Thus, it appears reasonable to use the same V_a^2 factors for both gases, namely the choice with β = 230 cm^{-1} that was selected for Ar.

There remains the factor $I(\Delta E)$, and it is here that we find the big difference between the two collision partners (see Figure 8), occurring principally on account of the reduced mass of the collision pair. The effect on the respective flow patterns is easy to predict. The restriction on large ΔE transfers with Ar is greatly relaxed for He. Thus, the He rate constant $k_4(8^1)$ (ΔE = 173 cm^{-1}) is much more competitive with $k_4(30^1)$ (ΔE = 119 cm^{-1}) than in the case of Ar collisions. This competition is the principal difference in the flow patterns of Figure 9. The large ΔE channels 17^1, 30^2, and 30^3 should also be more competitive for He. On this issue, the spectra in Figure 1 that compare He and Ar behavior suggest exactly the opposite. Those spectra are deceptive, however, in that they were obtained at relatively high added gas pressures to display the band positions clearly. Under those conditions, two- and three-collision sequences are important in establishing 30^2 and 30^3 populations, and the directed flow of VET into the $\Delta v_{30} = \pm 1$ channels for Ar (89% vs 59% for He) specially favors the buildup of those levels.

The comparisons of the SSH-T rules with experimental flow patterns for He-pDFB collisions are given in Table VIII and Figure 9. The replication of the data is rather good. Thus, the SSH-T model can reproduce well the sensitivity of the flow patterns to the differences in these collision partners.

The above discussion shows explicitly why He and Ar flow patterns should differ. The discrimination is entirely in the $I(\Delta E)$ factor and that in turn is caused by the differences in μ and, to a less extent, ϵ. We could find in these arguments a rationale for the impressive demonstration by Struve and co-workers[10] of common flow patterns for 0^0 aniline VET with many collision partners. None of their partners were light gases that could provide a big variation in μ or ϵ. The rationale runs into problems, however, on account of earlier aniline observations by Cameron, Vandersall, and Rice.[9c] They found qualitatively similar flow patterns for He and Ar. The picture is further clouded by benzene[5] whose flow patterns are similar for He and N_2 but not CO. No explanation emerges from the simple SSH-T model for these behaviors.

5. SSH-T Predictions without Correction for Collision Dynamics. The preceding discussions are based on the use of the SSH-T model as expressed in eq 11. This form contains the factors C_{if} that were introduced by McDonald and Rice[12] to account for geometric considerations of the collision dynamics that extend beyond those in the "breathing sphere approximation" first introduced by Tanczos.[30] In fact, the C_{if} factor remains as the only introduction of collision dynamics to our SSH-T treatment since we assume uniform A^2 factors among the vibrational matrix elements for various modes of pDFB. Those A^2 factors were the (modest) discriminations among modes in the breathing sphere treatment of Tanczos.

We have explored the data replications by the SSH-T model when the C_{if} factors are all set to unity in order to remove any sensitivity of the model to collision dynamics. The comparisons of this SSH-T form with the data are done as before. With $I(\Delta E)$ being that for a = 2.1 Å^{-1} via numerical integrations of Thompson's formula (see Figure 8) and β = 230 cm^{-1}, the SSH-T flow patterns are compared with the experimental data in Figure 9. The constant β = 230 cm^{-1} is common to both sets of rules (with and without C_{if}) since, in its determination using the ratio $k_4(30^1)/k_4(30^2)$, the C_{if} factors drop out.

The comparisons show that the Ar flow patterns are replicated with about equal fidelity with or without C_{if} factors.

In contrast to Ar, the SSH-T replication of the observed He flow patterns is substantially degraded by setting the C_{if} factors to a uniform value; see Figure 9. A much more discriminating test for the effect of the collision dynamics occurs, however, for energy transfer from higher S_1 levels. In other work[28] we have seen that the SSH-T modeling is much improved with C_{if} factors.

6. Comparison with Crossed-Beam S_0 Vibrational Energy Transfer. Hall et al.[21] have included pDFB among a series of molecules in which vibrational energy flow within the S_0 state is monitored when induced by He collisions. The experiments are pathfinders in polyatomic VET because they involve two unique conditions, both arising from the use of crossed molecular beams. (i) The center-of-mass collision energies are narrowly defined and can be selected over a range from tens of cm^{-1} to above 2500 cm^{-1}. (ii) The VET involves rotationally and vibrationally cold polyatomics.

Their S_0 pDFB experiments parallel those in this paper in that they probe vibrational excitation from the vibrationless level. Their S_0 He + pDFB(0^0) transfers show remarkable selectivity, even if judged by the selectivity of our S_1 300 K experiments. Only a single mode, ν_{30}, undergoes collisional excitation. As in the S_1 state, ν_{30} is the lowest frequency mode, but in the S_0 state, 30_1 (158 cm^{-1}) and 30_2 (316 cm^{-1}) are the first two vibrational levels above 0_0, and these are the only levels observed in the inelastic scattering. The collisional energies are sufficient to excite many other modes and levels.

The 300 K S_1 He + pDFB(0^0) transfers described in the present paper are in comparison ecumenical. The cross section for excitation of 8^1 is about half that for 30^1 and the cross sections for other modes (e.g. 17^1) are sufficiently large to at least compete with 30^2 and 30^3 even if we cannot measure them.

In addition to 300 K thermal averaging over collision energies, three major differences exist between the S_1 and S_0 experiments. They operate with different intermolecular potentials, the pattern of vibrational frequencies is substantially altered between the two states and, finally, the crossed molecular beam experiments probe vibrational energy transfer from pDFB molecules having a much smaller ensemble of initial rotational states.

Present information offers comment on some of these factors. The He–pDFB intermolecular potentials are almost certainly not much different in the two electronic states, and neither Clary's calculations[27] nor the SSH-T propensity rules are very sensitive to small changes in the potential. On the other hand, both Clary's calculation and the SSH-T rules show high sensitivity to the mode

(51) Freed, K. F. *Chem. Phys. Lett.* **1984**, *106*, 1.

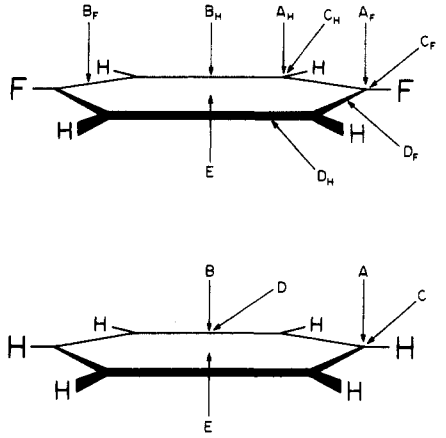

Figure 10. Representative collision trajectories used by McDonald and Rice[12] for benzene calculations (bottom) and those for this study on pDFB.

frequency (the latter in the $I(\Delta E)$ factor) for collisional excitation from the zero-point level. The relatively high frequency of other modes in S_0 as opposed to S_1 is probably the most critical difference in the two electronic states.

7. Is ν_{30} a "Special" Mode in Collisional Vibrational Energy Transfer? The mode ν_{30}, an out-of-plane fluorine bend against a rigid ring (see Figure 6), is the lowest frequency mode in both S_1 and S_0 pDFB. Hall et al.[21] see ν_{30} as the only mode undergoing change in their S_0 experiments. We see that it is the most active mode in S_1 VET. Further evidence for the domination of S_1 collisional flow by ν_{30} has been given elsewhere.[28]

Chemical timing studies show that the mode ν_{30} also plays a special role in collision-free intramolecular vibrational redistribution (IVR).[16,17,34,52] Those results are consistent with resolved fluorescence from higher S_1 pDFB levels showing that ν_{30} is specially effective in promoting mixing among S_1 levels.[18,19]

From these experiments, ν_{30} is seen to be a common accelerating mode for both collision-induced and collision-free vibrational energy flow. The former is driven by level mixing in the isolated molecule. Thus, it has been proposed[51] that the activity of ν_{30} in both processes might be evidence that isolated-molecule level mixing plays a dominant role in collisional transfers. That approach, however, has not yet led to even a qualitative account of the collisional VET.

Gentry and co-workers[21] have argued that the special role of ν_{30} in collisional transfers is due "simply to its low frequency and to a lesser extent its geometry". Clary's quantal scattering calculations[27] provide supporting insight to this proposition by the clever trick of repeating the S_0 calculations with the frequency of all six lower modes set at the ν_{30} value. With equal frequencies, the calculated cross sections for $v = 0 \rightarrow 1$ processes fall into two groups, out-of-plane vs in-plane modes. As expected, the out-of-plane cross sections are larger, but they exceed the in-plane values by only about a factor of 2. Thus, with $\nu_{30} = 157$ lying far below the next mode $\nu_{22} = 352$ cm^{-1}, the big factor for ν_{30} activity must be its low frequency.

For the S_1 state, ν_{30} dominance of VET in He + pDFB collisions is much reduced. In fact, another out-of-plane mode, ν_8, has $\Delta v = \pm 1$ cross sections only a factor of 2 below the ν_{30} values. When we look at the S_1 frequencies of these modes, we can perhaps see why both are so active. In the S_1 state, $\nu_{30} = 119$ and $\nu_8 = 173$ cm^{-1}. Their close values make a big contrast to the S_0 situation, where ν_{30} stands alone. The next S_0 fundamental, ν_{22}, is more than twice as large.

The story changes when we turn to S_1 VET with Ar collisions. Now the special nature of ν_{30} once again prevails, with the $\Delta v_{30} = +1$ cross section exceeding the next largest by about a factor of 6. As we showed in an earlier section on He + pDFB, the SSH-T model provides insights concerning why He and Ar collisions are so different. As ΔE rises above 100 cm^{-1}, the $(I\Delta E)$ scattering integral falls rapidly for Ar but not for He. In turn, that difference is chiefly generated by the distinctions in reduced mass as opposed to parameters of the interaction potential.

If we explore further the SSH-T model in eq 11 for ν_{30} activity in the Ar system, we see that there is a favorable confluence of all three SSH-T factors. The C_{if} factors discriminate terminally against in-plane modes but only modestly if at all among the out-of-plane modes. The V_a^2 matrix element has a $1/\nu$ dependence on mode frequency that most favors ν_{30} activity (a factor of ≈ 1.5 for ν_{30} vs ν_8). The largest contributor, however, is the scattering integral $I(\Delta E)$ that reflects mode frequencies indirectly by its dependence on ΔE, the $T \rightarrow V$ energy exchange. This factor boosts ν_{30} activity over that of its nearest rival ν_8 bu about a factor of 3 (see Figure 8).

TABLE IX: Projections of the Normal Modes of pDFB onto the Trajectories Shown in Figure 10

collision type, γ	$w(\gamma)$	projection, χ_a
A_H	0.01	$\chi_8 = 0.67$, $\chi_{16} = 0.47$
		$\chi_{30} = 0.28$, $\chi_9 = 0.49$, $\chi_{15} = 0.03$
A_F	0.05	$\chi_{29} = 0.67$, $\chi_{16} = 0.47$
		$\chi_{30} = 0.28$, $\chi_{17} = 0.47$, $\chi_{15} = 0.03$
B_H	0.05	$\chi_{29} = 0.82$, $\chi_{30} = 0.45$
		$\chi_9 = 0.34$, $\chi_{28} = 0.12$
B_F	0.10	$\chi_8 = 0.82$, $\chi_{30} = 0.45$
		$\chi_{17} = 0.34$, $\chi_7 = 0.45$
C_H	0.20	$\chi_8 = 0.47$, $\chi_{16} = 0.33$, $\chi_6 = 0.52$
		$\chi_{14} = 0.17$, $\chi_{20} = 0.06$, $\chi_5 = 0.05$
		$\chi_{15} = 0.52$, $\chi_{28} = 0.17$, $\chi_{30} = 0.03$
C_F	0.10	$\chi_{29} = 0.47$, $\chi_{16} = 0.33$, $\chi_{26} = 0.52$
		$\chi_{14} = 0.17$, $\chi_{20} = 0.06$, $\chi_{25} = 0.05$
		$\chi_{15} = 0.52$, $\chi_{28} = 0.17$, $\chi_{30} = 0.03$
D_H	0.10	$\chi_{29} = 0.47$, $\chi_{16} = 0.33$
		$\chi_6 = 0.56$, $\chi_5 = 0.14$
		$\chi_{30} = 0.45$, $\chi_9 = 0.34$, $\chi_{28} = 0.12$
D_F	0.20	$\chi_8 = 0.47$, $\chi_{16} = 0.33$
		$\chi_{26} = 0.56$, $\chi = 0.14$
		$\chi_{30} = 0.45$, $\chi_{17} = 0.34$, $\chi_7 = 0.12$
E	0.10	$\chi_{30} = 1.0$

Note Added in Proof. At about the time our manuscript was submitted, there appeared a report by Kable and Knight[53] concerning state-to-state VET in S_1 naphthalene (48 vibrational modes) induced by very low energy collisions with argon. The low collision energies were achieved by observing VET occurring in the collisional regime of a supersonic expansion of naphthalene seeded in argon. These low-temperature experiments bear on some issues discussed in our 300 K pDFB + Ar work. The paper also includes discussion of the time-dependent kinetics of VET in long-lived S_1 molecules as an alternative to the steady-state approach.

An earlier exploration of very low energy collision-induced VET in benzene-d_6 was carried out by similar methods.[54] Among other findings, it shows similarities in branching patterns to those of 300 K experiments. The low-temperature studies also revealed clearly the special nature of very light collision partners that is seen in our 300 K pDFB + He data.

Acknowledgment. Financial support from the National Science Foundation is greatly appreciated as is that from the NATO Collaborative Research Grants Program, Grant SA.5-2-05 (RG.0215/89). Comments from an alert referee were helpful.

Appendix: Collisional Coupling Terms

We assume the same molecular shape of benzene used by McDonald and Rice[12] in computer simulations of collisions with molecules (or atoms). By use of group theoretical arguments, the effect on each benzene normal mode by each collision trajectory deemed important (see Figure 10 for representative trajectories)

(52) Dolson, D. A.; Holtzclaw, K. W.; Moss, D. B.; Parmenter, C. S. *J. Chem. Phys.* **1986**, *84*, 1119.

(53) Kable, S. H.; Knight, A. E. W. *J. Chem. Phys.* **1990**, *93*, 4766.

(54) Rainbird, M. W.; Webb, B. S.; Knight, A. E. W. *J. Chem. Phys.* **1988**, *88*, 2416.

was assessed in the form of the projection χ_a^γ of ν_a onto the collision trajectory, γ. These factors are incorporated into a collisional coupling term, C_{if}, for transfer from level i to level f.

$$C_{if} = \sum_\gamma w_\gamma \Pi(\chi_a^\gamma)^{2\Delta v_a}$$

Here w_γ is the geometrical weighting factor for collision trajectory γ (shown in Figure 10).

The collisional coupling term takes the place of the sum over surface atom displacements in the vibrational matrix element and fits into the propensity rules as another multiplicative factor.

In applying this model to pDFB, we assume the geometrical shape drawn for benzene. Figure 10 shows the representative collision trajectories chosen for pDFB by direct comparison to those chosen for benzene by computer simulation. Simple symmetry arguments were used to translate the "benzene trajectories" into "pDFB trajectories".

Consider the collision trajectories B_H and B_F (degenerate trajectories in the benzene case), both out-of-plane trajectories impinging on the carbon–carbon bonds as shown in Figure 10. These clearly have different weighting factors and, in fact, $w(B_F) = 2w(B_H)$ because there are twice as many "targets" for B_F than for B_H. The sum of $w(B_F)$ and $w(B_H)$ should equal the value of $w(B)$ for benzene, i.e., $w(B) = 0.15$. Thus, $w(B_H)$ and $w(B_F)$ are 0.05 and 0.10, respectively.

Collision type B in benzene affects the doubly degenerate mode 10 and χ_{10}^B is 0.34. Mode 10 is not degenerate in pDFB but splits into ν_9 (10a) and ν_{17} (10b). They will be affected by collision trajectories B_F and B_H, respectively. Normal vibrations 9 and 17 are shown in Figure 6. A collision trajectory impacting pDFB on the carbon–carbon bond (where both carbons are attached to a hydrogen) may induce atomic displacements along normal mode 9 while not inducing displacements along normal mode 17. The converse is true for a trajectory impacting the pDFB on a carbon–carbon bond where one carbon is attached to a fluorine, B_F. Thus, we assign the following projections for pDFB.

$$\chi_9^{B_H} = 0.34 \qquad \chi_9^{B_F} = 0.00$$

$$\chi_{17}^{B_H} = 0.00 \qquad \chi_{17}^{B_F} = 0.34$$

The trajectory projections for the other normal modes shown in Figure 10 were determined in a comparative manner and are collected in Table IX. The resulting collisional coupling terms for $\Delta v = 1$ changes in all 30 normal modes are given in Table VI.

Registry No. pDFB, 540-36-3; Ar, 7440-37-1; He, 7440-59-7.

Intramolecular Hydrogen Bond in the Ground and Excited Electronic States of 2-Hydroxyquinoline. A Study Using High-Resolution Laser Spectroscopy

A. Held, D. F. Plusquellic, J. L. Tomer, and D. W. Pratt*

Department of Chemistry, University of Pittsburgh, Pittsburgh, Pennsylvania 15260
(Received: October 9, 1990)

2-Hydroxyquinoline (2HQ) is known to exist in two tautomeric forms, the lactim ("enol") and lactam ("keto"), which exhibit different electronic spectra. Reported herein are spectra of the isolated molecule at full rotational resolution which show (1) that the higher frequency electronic origin is that of the lactim form, (2) that in the ground electronic state (S_0) the more stable rotamer of the lactim has an O–H bond that is cis with respect to the naphthalene frame, (3) that this rotamer exhibits an out-of-plane intramolecular hydrogen bond involving the OH group and the ring nitrogen, and (4) that on electronic excitation of this rotamer to the S_1 state there is only a small shift of the hydroxy hydrogen toward the nitrogen atom. Additionally, it is found (5) that the $S_1 \leftarrow S_0$ transition is mainly long-axis polarized, demonstrating that the S_1 state is principally $\pi\pi^*$ in character. The interpretations of these results and their implications for the acid–base properties of 2HQ in both electronic states are discussed.

Introduction

In the introduction to their classic text, *The Hydrogen Bond*, Pimentel and McClellan state that "it is hardly an exaggeration to say that in the chemistry of living systems the hydrogen bond is as important as the carbon–carbon bond."[1] Later, describing the application of different spectroscopic techniques to hydrogen-bonded substances, they note that "it is to be expected that the UV–visible spectrum of a molecule may be altered by the formation of a hydrogen bond if the chromophoric portion of the molecule is perturbed."[2] And, still later, they point out that changes in such spectra "furnish the only experimental evidence available concerning the hydrogen-bonding properties of electronically excited states."[3] These remarks are as true today as they were 30 years ago. Thus, in honoring the memory of George Pimentel with this special issue, it seems appropriate to focus on one molecule in which there is an intramolecular hydrogen bond, 2-hydroxyquinoline, and to show how the properties of this bond in both the ground and an excited electronic state are revealed by high-resolution optical spectroscopy in the gas phase.

2-Hydroxyquinoline (2HQ), a weak base in its electronic ground state, is known to exist in two tautomeric forms, the lactim (2-quinolinol, I) and the lactam (2-quinolinone, II). The two forms

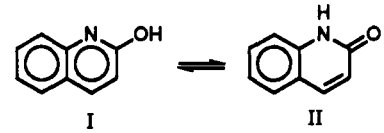

I II

are related by H-atom transfer from or to the oxygen atom to or from the ring nitrogen. Additionally, the lactim exhibits rotational isomerism, there being two possible orientations of the O-H bond with respect to the naphthalene frame, *cis*-(Ia) and *trans*-(Ib).

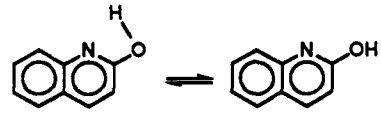

Ia Ib

Of the two tautomers, the lactim (I) is slightly (~1 kJ/mol)[4] more

(1) Pimentel, G. C.; McClellan, A. L. *The Hydrogen Bond*; W. H. Freeman: San Francisco, 1960; p 9.
(2) Pimentel, G. C.; McClellan, A. L. *The Hydrogen Bond*; W. H. Freeman: San Francisco, 1960; p 157.
(3) Pimentel, G. C.; McClellan, A. L. *The Hydrogen Bond*; W. H. Freeman: San Francisco, 1960; p 164.

0022-3654/91/2095-2877$02.50/0 © 1991 American Chemical Society